A Study of Relative Efficiencies of Photomultiplier Tubes in the Sudbury Neutrino Observatory

by

Christian Van Ouellet

A thesis submitted to the Department of Physics
in conformity with the requirements
for the degree of Master of Science

Queen's University
Kingston, Ontario, Canada
August, 2003

ABSTRACT

The Sudbury Neutrino Observatory (SNO) is a spherical heavy water Cerenkov-light detector built to understand neutrino physics. In particular it is credited with solving the "missing" solar neutrino problem. The SNO project uses a laser light with a diffuser, called a "laserball", to determine all the optical properties of the SNO detector from attenuation lengths in the water to individual photo-multiplier tube (PMT) characteristics. One such characteristic is the quantum efficiency, and it is the purpose of this study to investigate this quantity. A characteristic of laserball data is that one does not measure quantum efficiency but rather relative efficiencies. This thesis is a systematic analysis of the efficiencies extracted from pre-existing calibration code. Knowing the relative efficiencies increases the understanding of the detector's behavior in a previously unexamined area. Introduction of the PMT-to-PMT variations in efficiency into the pre-existing mathematical Monte-Carlo model of SNO has demonstrated better agreement between the observed and modeled energy resolution of the detector. The implications of this last Monte-Carlo adjustment may impact current published SNO results and further constrain theoretical models for neutrino oscillations.

ACKNOWLEDGEMENTS

I would like to thank the very many people who have contributed to the success of my thesis and in particular:

1. My advisor, Aksel Hallin, who has taught me more about experimental science in 2 years then I learned in all my previous education. However the most important thing he has taught me is self motivation and that was certainly the hardest lesson to learn.

2. Hamish Leslie, without whome I would likely never had entered experimental science. His poingnant skepticism and subtle wit was always helpful and well received.

3. Jose Maneira for his patience that knows no bounds. His insight permeates the largest portions of my thesis without which, would be still a year in the works if at all.

4. Art McDonald, who has the very tall order of keeping the entire ship afloat. Art made me feel like a part of the collaboration rather than just another Master's student and I really appreciate it.

5. Vera Tang who stuck with me through it all. She really deserves a medal but will have to settle for a ring.

6. My hard working mother who taught me the value of education above all else and my philosophical father who keeps the other half of my brain entertained.

7. Phil Harvey who at the last moment bailed me out of many situations best described by Murphy's Law.

8. Peter Skensved always came through when computer problems arose (which were many). His insight into cross-checks is well appreciated.

9. The many grad students I've come to know and work with over the years most notably Marcus Thompson and Mark Kos.

This thesis is dedicated to Waar and Mroo who taught me the meaning of hubris and its worst consequence.

CONTENTS

LIST OF FIGURES

LIST OF TABLES

1. INTRODUCTION

A photomultiplier tube (PMT) is a device used to detect light. The principle behind the detection mechanics is as follows. An incident photon strikes a plate which ejects an electron from the plate - the photo-electric effect. This electron is then accelerated toward a secondary metal plate via an electric field. The electron gains energy in its transit and when it strikes the secondary metal plate it causes a number of electrons to be ejected. These electrons are then accelerated toward a tertiary plate, which each eject a number of electrons that are accelerated to a fourth plate. This process continues until enough electrons are created for a measurable pulse from a single photon interaction. Because of various physical constraints, from the geometry of the electric field to the geometry of the plates, an incident photon does not always result in an observed pulse. Quantum Efficiency (QE), more specifically the responsive quantum efficiency, is defined as the wavelength dependent ratio of the number of pulses produced by the PMT to the number of incident photons. QE would be a readily measured quantity if one were able to fire a known number of photons incident on the PMT and simply tabulated the PMT pulses registered. In the case of the laserball the number of photons emitted per pulse is not known precisely and thus QE is not easily measured. The laserball data is modeled in such a way that of the many unknown optical parameters, the QE of a given tube is factored out. Once all other optical parameters have been found through fitting data to theory, QE can then be calculated from the model fits. As will be seen, QE can never truly be disentangled from a multiplicative factor, but PMT

to PMT comparisons produce a relative efficiency. The details of this procedure are described in the next section.

1.1 The Optical Model

The optical model, detector, and source specifics are discussed in detail in Bryce Moffat's PhD thesis [1]. Only the necessary introduction is provided here.

A very simplified description of the SNO detector and calibration follows. SNO is essentially a 6 meter radius sphere of heavy water (D_20) surrounded by light water (H_20) with acrylic at the interface. The acrylic is roughly 5.5 cm thick and referred to as the "acrylic vessel" (AV). Nine meters from the center of the heavy water sphere is a shell of 9522 PMTs and reflectors pointed toward the center, mounted on a stainless-steel PMT support structure (PSUP). The acrylic interface forms at the top of the sphere into a 70 cm radius cylindrical chimney that extends into an operations room called the "deck". It is through this chimney that various calibration sources are lowered into the heavy water. The laserball is one such source. At its simplest the laserball can be described as a diffusion bulb at the end of a fiber optic cable [2]. The diffusion bulb is a spherical glass container filled with a silicone gel suspension of 50 μm glass beads. When the laser is pulsed from the deck area the light travels down the fiber and is scattered isotropically by the beads. In a calibration event some portion of the scattered laser light travels through the water and acrylic of the detector to impact on a PMT.

The optical data taken for calibrations using the laserball is organized in sets of closely spaced "runs" of roughly 15 minutes each, taken over the course of several days. Collectively these runs are referred to as a "scan". The laser outputs 337.1 nm wavelength light and scans are made at 386, 420, 500 and 620 nm by placing an appropriate dye cell in the laser path to shift the wavelength. During a run the laserball is held fixed in position. The laserball can

be positioned at various points in the detector via a rope manipulation system allowing for off-center calibration data. Over the course of a scan the operators endeavor to acquire as many positions as time permits in the detector schedule at all of the wavelengths. At each wavelength there are always a few runs taken with the laserball in the center of the detector that are termed "central runs" and these are critical to the calibration effort. There is no fixed number of runs at a given wavelength in a given scan, they vary usually from about 20 to around 40. There are currently three principal calibration scans, September 2000, September 2001 and May 2002. One important thing to note is that September 2000 and September 2001 data were taken with pure D_20 in the detector and May 2002 data were taken when salt was added to the D_20 to enhance the neutrino-deuteron interaction.

The light collected from a single event in the detector comes in bursts separated in time by well understood delays. The first and largest burst is termed the "prompt" burst and arrives at the PMTs without reflection from anything other than the given PMT's reflector. This thesis only concerns itself with prompt light. The prompt intensity N_{ij} observed in PMT j for a run i is parametrized as follows :

$$\mathbf{N_{ij} = N_i \Omega_{ij} R_{ij} L_{ij} T_{ij} \epsilon_{ij} e^{-(d_d \alpha_d + d_a \alpha_a + d_h \alpha_h)}}$$

$\mathbf{N_i}$ is the number of photons emitted by the laserball in run i and detected within a prompt timing window at each PMT. This is the intensity normalization and it cannot be measured directly with great precision.

$\mathbf{\Omega_{ij}}$ is the solid angle of PMT j for run i, the acceptance. This number can be calculated from geometry.

$\mathbf{R_{ij}}$ is all other geometric factors beyond solid angle. This needs to be measured due to the complexity of the geometry of each individual PMT.

$\mathbf{T_{ij}}$ are the Fresnel transmission coefficients for the heavy-water/ light-water/acrylic interfaces. This number can be calculated from theory.

$\mathbf{L_{ij}}$ is the laserball light distribution, $L(cos(\theta), \phi)$. Theta is the plane-polar angle and phi is the z-direction polar angle with z defined as the axis going through the neck of the detector and the origin at the center of the detector. This number needs to be measured.
$\mathbf{d_a}$, $\mathbf{d_d}$ and $\mathbf{d_h}$ are the distances of the light paths through the acrylic, the D_2O and the H_2O respectively. These numbers can be calculated from geometry.
αs are the attenuation coefficients in the respective media. These numbers need to be measured.

It is $\epsilon_{\mathbf{ij}}$, the QE of tube j in run i, which is the quantity of interest in this study.

1.2 The Occupancy Ratio Method

The occupancy of a PMT j for run i is defined as the ratio of prompt PMT pulses detected over pulses of the laser for that PMT:

$$(OCC_{raw})_{ij} = (\frac{N_{prompt}}{N_{pulses}})_{ij}$$

This number is then corrected assuming Poisson statistics of the rare occurrence of multiple photoelectrons (MPE) being detected from a single laser pulse simultaneously. The pulse width of the laser is 600 ps. The MPE corrected prompt occupancy is:

$$(OCC_{prompt})_{ij} = (-ln(1 - OCC_{raw}))_{ij}$$

The number of prompt photons $N^{MPE}_{prompt} = N_{pulses} OCC_{prompt}$ is then identified with the prompt intensity of the optical model,

$$(N^{MPE}_{prompt})_{ij} = N_{ij}$$

The SNO detector is spherical and thus the geometry lends itself well to calibrations from the central point. The principle of the occupancy ratio method

is to compare the occupancy found with the laserball at various positions in the detector with a central run occupancy. The subscript "0" denotes a central run number.

Terms that can be calculated purely from source position geometry can be corrected for in the data at this level:

$$OR_{ij}^{data} = \frac{N_i}{N_0}(\frac{\Omega_{0j}T_{0j}}{\Omega_{ij}T_{ij}})$$

while the optical model occupancy ratio is:

$$OR_{ij}^{model} = \left(\frac{N_i}{N_0}\right)\frac{R_{ij}L_{ij}}{R_{0j}L_{0j}}e^{\delta d_d\alpha_d+\delta d_a\alpha_a+\delta d_h\alpha_h}$$

where $\delta d = d_{ij} - d_{i0}$ is the path difference in the respective media. Optical parameters are then determined by minimization of the chi-square difference between the data and the model:

$$\chi^2 = \sum_i^{N_{runs}}\sum_j^{N_{PMT}}\frac{(OR_{ij}^{data} - OR_{ij}^{model})^2}{(\Delta OR_{ij})^2 + \sigma_{PMTij}^2}$$

where ΔOR_{ij} is the statistical uncertainty in the occupancy ratio due to counting statistics and σ_{PMTij}^2 is an additional uncertainty introduced to account for PMT response variability on the incidence angle of the light.

1.3 The Efficiency Calculation

It is important to note that when the occupancy ratio is taken the unknown PMT QEs, ϵ_{ij}, drop out. After the fits the values of R_{ij}, L_{ij}, and the various attenuations α_xs are known. If we look at the original equation for the prompt intensity N_{ij},

$$N_{ij} = N_i\Omega_{ij}R_{ij}L_{ij}T_{ij}\epsilon_{ij}e^{-(d_d\alpha_d+d_a\alpha_a+d_h\alpha_h)}$$

then the only terms remaining that are unknown are N_i and ϵ_{ij}. However, the chi-square minimization of the fit also returns values for the ratio of $(\frac{N_i}{N_0})$ and

thus by dividing both sides of the equation by this known value the N_i cancel out leaving a number $N_0\epsilon_{ij}$ which is a **run-independent measure of the QE** for any tube i in run j inside the same scan.

$$N_0\epsilon_{ij} = (\frac{N_0}{N_i})\frac{N_{ij}e^{(d_d\alpha_d+d_a\alpha_a+d_h\alpha_h)}}{\Omega_{ij}R_{ij}T_{ij}L_{ij}}$$

1.4 The Efficiency Used and the Error on the Efficiency

The number $N_0\epsilon_{ij}$ being used in this analysis is taken from one of many methods in the QOCA code (QOCAPmt->Geteffm()) developed by B.Moffat and M.Boulay [1] [4] It is of great importance that this number be well understood. The number $\frac{N_0}{N_i}$ produced by the function is always a number on the order of unity. This is because N_0 and N_i are always roughly of the same order of magnitude, the runs always being roughly the same length (15 min). Because the fits can not seperate N_0 from N_i, only the ratio of the two, the code simply sets N_0 to the first ratio of $N_0/N_{i=1}$. For comparison purposes this is an irrelevant scale factor and a given PMT efficiency extracted from the code will be scaled to the average efficiency of all PMTs in the scan to yield a distribution centered about 1. The error in the efficiency is initially estimated as a group of optical constants β times an occupancy, N_{ij}. As a counting experiment, the error that is used is then $\Delta N_0\epsilon_{ij} = \beta N_{ij}^{1/2}$. The error will be revised and discussed in greater detail in the following chapter.

2. CONSISTENCY OF THE EFFICIENCY CALCULATION

The first question that begs an answer is "How good is the measure of efficiency?" considering the number obtained for efficiency is dependent on all other model parameters.

2.1 Run to Run Comparison Inside a Scan

The data gathered from SNO, be it calibration data or otherwise, is written to magnetic storage tapes in a format called "ZDABS", which labels runs in a 10-digit number format. The laserball calibration runs are organized into trees, called OCA trees, according to wavelength and scan, and have their own scheme for run index. There are many schemes for numbering PMTs. The OCA code has a numbering scheme where only PMTs that have produced pulses from laser light are tabulated. These tubes are refered to as having "occupancy". Logical channel number (LCN) is yet another scheme that is related to the electronics numbering of the data acquisition system in single file. The electronics numbering is in the form of crate/card/channel, where crate ranges from 0-18, card from 0-15, and channel from 0-31. Thus LCN 0 corresponds to 0/0/0, LCN 32 corresponds to 0/1/0 and LCN 512 to 1/0/0 and so forth. The analysis and graphs presented are in this LCN ordering.

The laserball data are organized in a two dimensional histogram, figure.2.1. The run index is along the x-axis versus the PMT LCN on the y-axis. Each

bin is weighted by the efficiency and the efficiency error calculated as detailed previously.

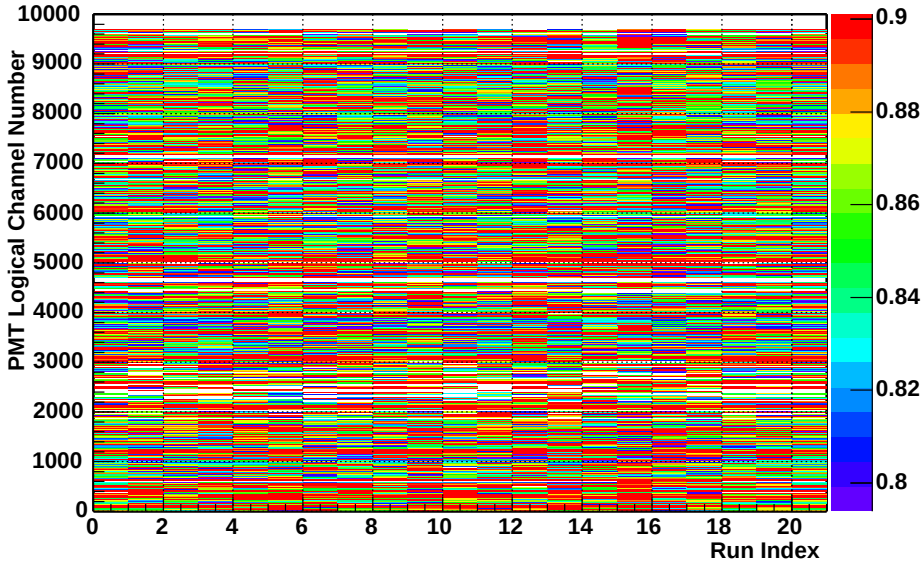

Figure 2.1: PMT efficiency displayed according to OCA run index and LCN September 2000 420nm

The efficiency for each PMT as a function of run index is then fitted to a flat line. Examples can be seen in figure.2.2 and figure.2.3. The "fitted efficiency" for each PMT is then the height of the flat-line fit and these are tabulated in figure.2.4.

The chi-square values of the flat line fit are similarly graphed and tabulated in figure.2.5, giving a measure of goodness of fit. For a good fit with 20 degrees of freedom one would want something on the order of 20 for chi-square. This means a chi-square per degree of freedom, also called "reduced chi-square", on the order of 1. This is clearly not always the case, however before jumping to any conclusions it becomes important to discuss relevant cuts made to the data and systematic errors.

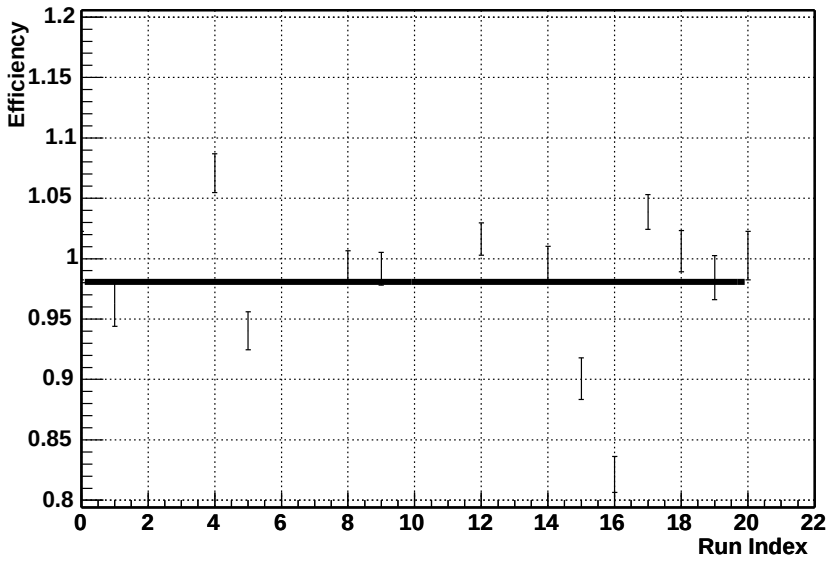

Figure 2.2: PMT number 2204, September 2000 420 nm. Chiquare is 15.3

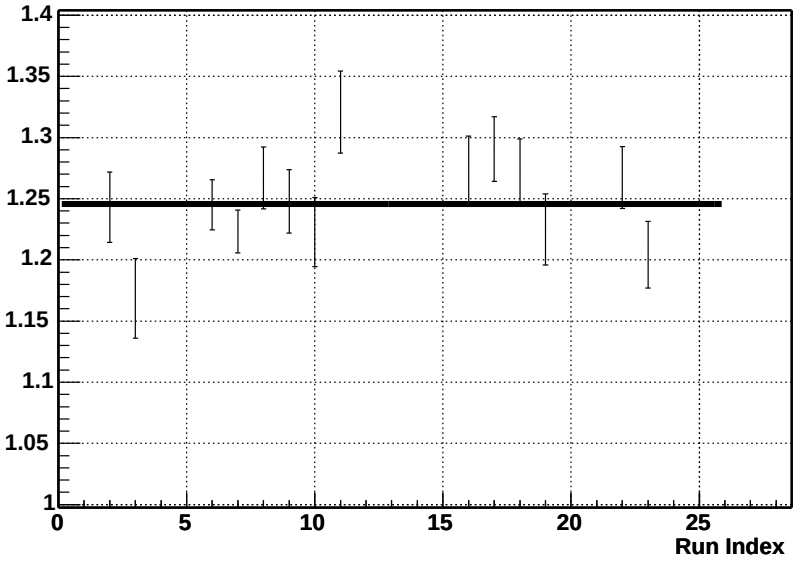

Figure 2.3: PMT number 254, May 2002 420 nm. Chisquare is 3.0

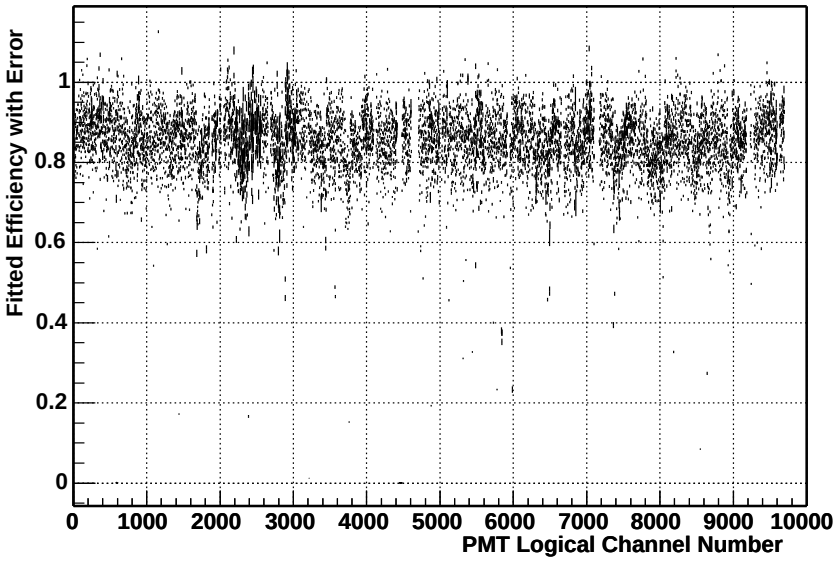

Figure 2.4: Fitted efficiency for each PMT with errors, September 2000 420 nm

2.2 PMT Selection

SNO has 9453 inward facing "normal" PMTs, 91 "owl" or outward looking PMTs, 49 low-gain PMTs, 22 butt PMTs, and 4 neck PMTs. This thesis is restricted to the 9453 normal inward facing PMTs, the others are simply not significant to this study and won't be discussed. There are a number of optical difficulties to be taken into account for in the calibration of the detector. Chief among concerns is that the AV which separates the heavy water from the light water is held up by an array of ropes attached to reinforced acrylic sections of the vessel called belly plates. There are also pipes for D_2O recirculation to ensure water purity that stretch the length of the vessel. The PMTs are affixed to a support structure just beyond the AV in the light water and thus the ropes, belly plates, and pipes lie in their way. These PMTs which have known poor calibrations based on central run optics correspond to about 23% of the total

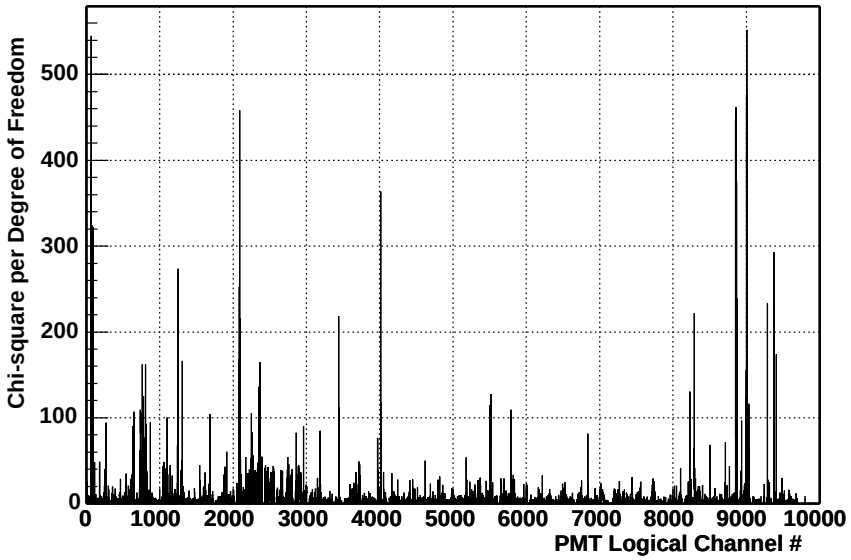

Figure 2.5: Chi-square per degree of freedom for the flat line fits for each PMT, September 2000 420 nm

detector's phototubes and their impact can be clearly seen in figure.2.6.

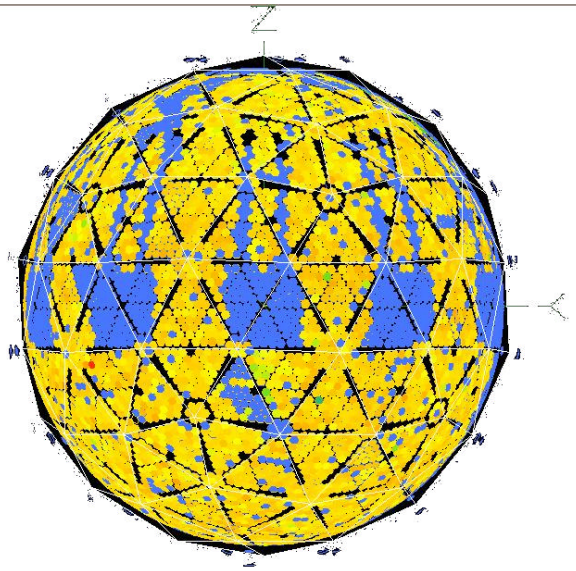

Figure 2.6: PMTs without geometric difficulties are shown in yellow. Belly plates and ropes are clearly visible in blue. This picture was generated from central run optics. The belly plates and ropes can be calibrated using off-central run optics.

For each run each PMT has a label called fBad which distinguishes the PMT as having poor calibration properties due to the run's laserball position. An fBad of 0 or 10 is acceptable, 1 or 11 is not. fBad equal to zero means the PMT can be calibrated from purely the central run. fBad equal to eleven means the PMT can be calibrated from off-central runs. fBad of 10 means the PMT calibrates well for non-central positions of the laserball. If a PMT has fBad of 1 or 11 for a given run, this flags that during that given run that PMT should not be considered as having proper calibration optics. If the flat line fits to the data are performed without cutting out PMT efficiencies on runs where fBad is 1 or 11, then a significantly poorer fits result. The fit is particularly poor for the PMTs that only calibrate with off-central runs such as PMTs shadowed

by belly plates and pipes. The impact of cutting on fBad for chi-squares of the flat line fit for each PMT is readily visible in the graphical displays: figure.2.7, figure.2.8, figure.2.9 and figure.2.10.

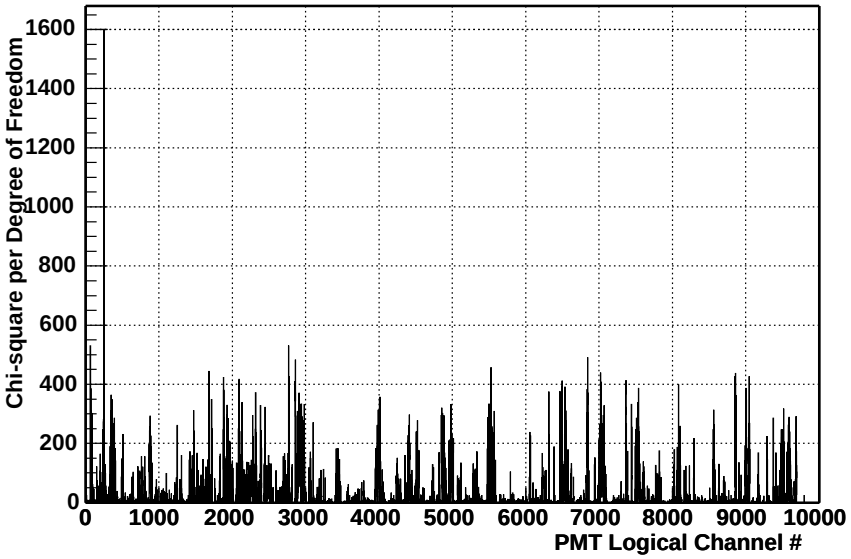

Figure 2.7: Reduced chi-square for the flat line fits to the PMT's efficiency with no fBad cuts

2.3 Systematics

Eight systematics have been investigated that can contribute to error in the efficiency measurement. These are the same systematics Bryce Moffat used in testing the various optical model parameters [1]. The method is to perform the optical model fits on the data with an artificially introduced error in one parameter and then to compare the resultant efficiencies to the nominal data fit's efficiencies analyzed throughout this thesis.

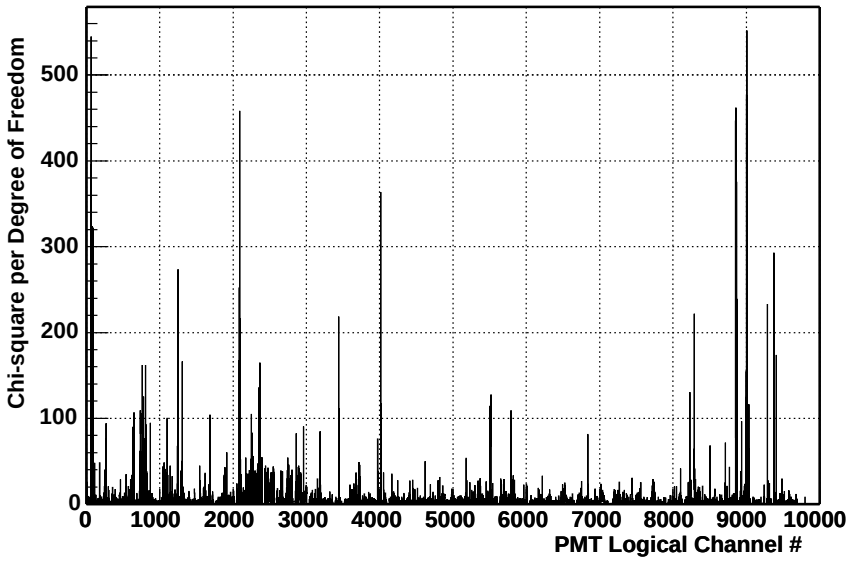

Figure 2.8: Reduced chi-square for the flat line fits to the PMT's efficiency with fBad cuts

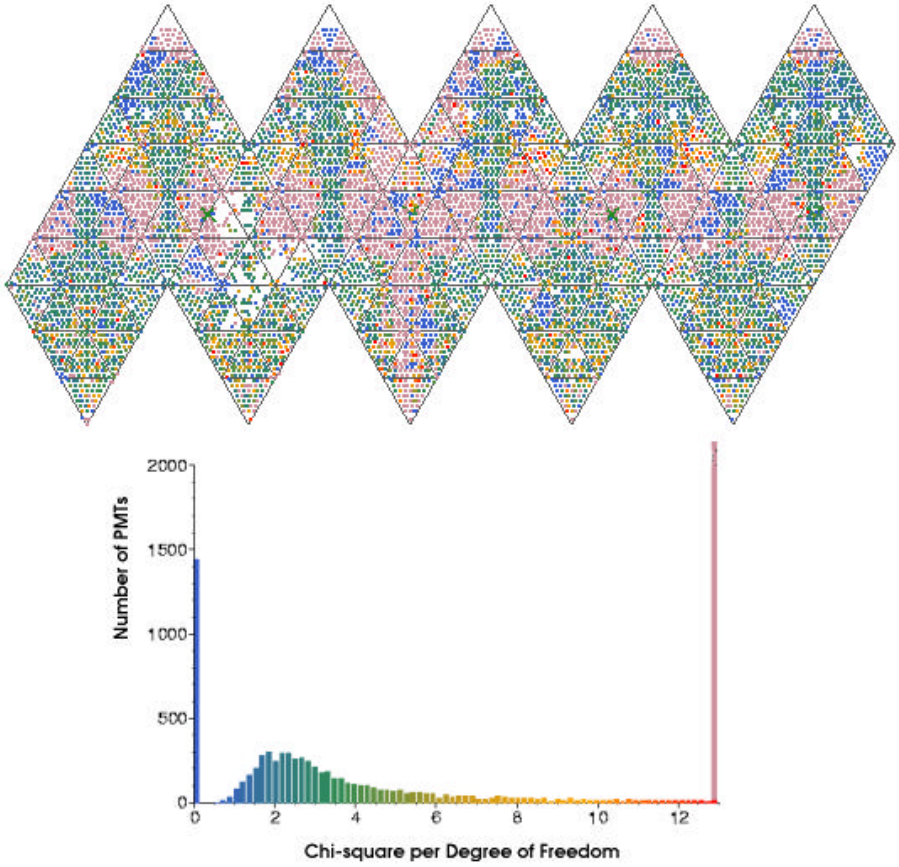

Figure 2.9: The detector is unwrapped here, not unlike an orange, and shows the reduced chi-square of the flat line fit to the PMT's efficiency in the PMT's physical position in the detector. In this case there are no cuts on fBad. The colors in the histogram are the very same on the detector folded out above it.

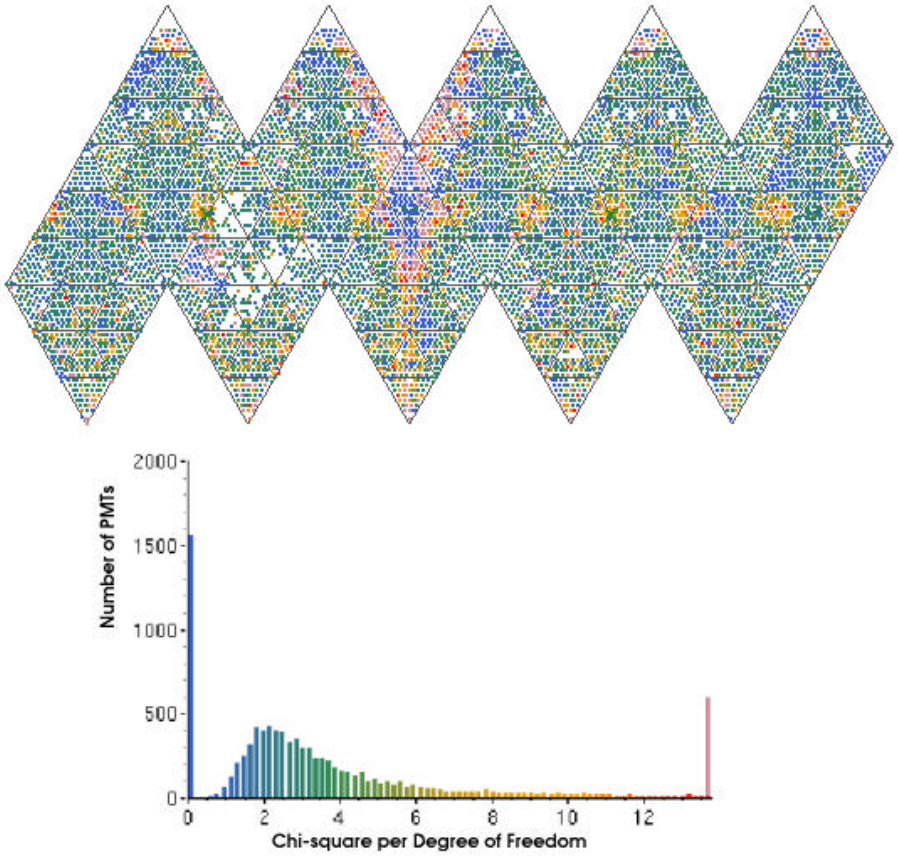

Figure 2.10: Identical situation as the previous graph but with cuts on fBad. There is notable sharpening of the detector features that create optical difficulties such as the belly plates. A better fit is clearly achieved for more PMTs by cutting on fBad as can be seen in the shift of previously high chi-square PMTs towards lower chi-square values. The colors in the histogram are the very same on the detector folded out above it.

1. **Radial scale shift** R' = 1.01 R. This can be roughly equated to an underestimate of the group velocity of photons at the laserball level.

2. **Z position shift** Z' = Z + 5 cm. A laserball position shift may be the result of the manipulator system reporting the incorrect laserball position or some other calibration being off.

3. **X position shift** X' = X + 5 cm.

4. **Radial position shift** R' = R + 5 cm.

5. **Radial position smear** R' = R + Gaus(σ = 5 cm). The laserball positions are displaced by a random amount sampled from a Gaussian of 5 cm width centered at zero in any given run. This systematic accounts for random inaccuracy in laserball position across runs.

6. **Laserball-PMT distance shift** Labeled L_d in the table. The distance from the laserball to each PMT was decreased by 3 cm. This accounts for the finite size of the laserball (10 cm radius). The light is in reality emitted closer to the PMTs on average.

7. **Flat laserball distribution** The laserball light distribution was forced to be flat. L(cosθ,ϕ) = 1.

8. **Laserball distribution squared** The laserball light distribution is forced to be the square of the laserball distribution calculated from the systematics-free fits. L(cosθ,ϕ) = (L(cosθ,ϕ)$_{free}$)^2

Systematic			
	without correction	correction factor	corrected
R' = 1.01 R	0.122557	0.20	0.0245114
Z' = Z + 5 cm	0.123802	0.40	0.0495208
X' = X + 5 cm	0.135807	0.40	0.0543228
R' = R + 5 cm	0.134821	0.20	0.0269642
R' = R + Gaus(σ = 5 cm)	0.122557	0.20	0.0245114
L_d	0.130698	0.50	0.0653490
L(cosθ,ϕ) = 1	0.125652	0.05	0.0062826
L(cosθ,ϕ) = (L(cosθ,ϕ)$_{free}$)^2	0.146529	0.05	0.0073264

Table 2.1: Evaluated systematic errors of the fitted efficiency

The effects of these systematics on the fitted efficiencies for PMT i, ϵ_i^f are calculated as an average ratio:

$$\frac{\sum_{i=0}^{i=N_{PMT}} \frac{\epsilon_i^f - \epsilon_{isystematic}^f}{\epsilon_i^f}}{N_{PMT}}$$

These results are summarized in table.2.1.

The systematics calculated are overestimates. Scaling these systematics by a correction factor they are made more reasonable, as described in detail in B.Moffat's thesis [1]. Position changes result from comparison between manipulator coordinates and optical position fit coordinates. The mean change is roughly 1±1.5 cm and 0.4±1.9 cm radially. B.Moffat assigns a conservative 5% uncertainty in the laserball distribution from his analysis and that is what is used in this thesis as well. For a global systematic error, the square root of the sum of the squares of systematics is taken. Only the highest laserball systematic, the squared distribution, is factored into the global systematic. The global systematic error is 10.8%.

This global systematic error is then summed in quadrature with the statistical error for each efficiency and the fitted efficiency is recalculated. Adding the global systematic error does not change the fitted efficiency value but does improve the chi-square. Returning to the poor fit shown in figure.2.2 the effective larger error bars can be seen in figure.2.11.

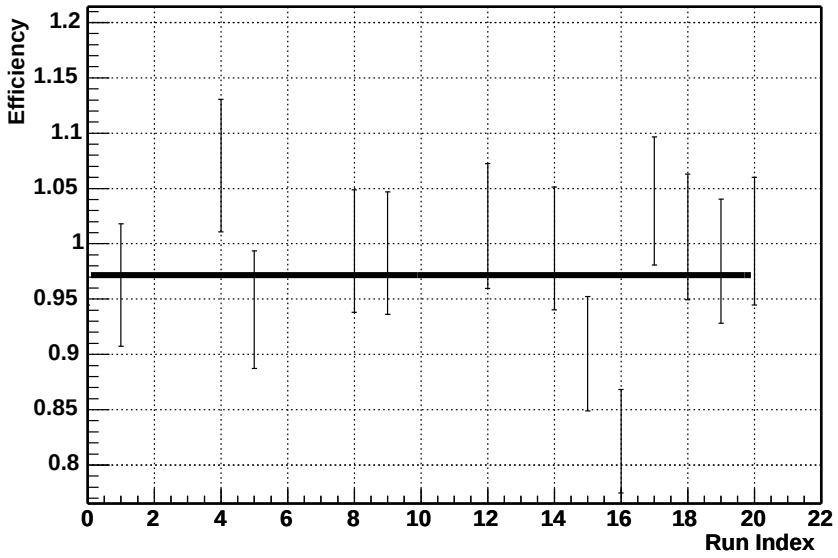

Figure 2.11: PMT number 2204, September 2000 420 nm, with clear outlying efficiencies despite the systematic error being factored into the error along with the statistical error. Chisquare is 1.8

The reduced chi-square distribution of the fits is shifted lower by the increase in error as seen in figure.2.12. The chi-square distribution is centered below 1, which is an indication that the systematic errors are correlated. The nature of the correlation has yet to be investigated.

There is a trend in the data that can be seen in the pronounced tail of the chi-square distribution toward higher chi-square values. This is true even with statistical and systematic errors contributing as uncorrelated-correlated to the

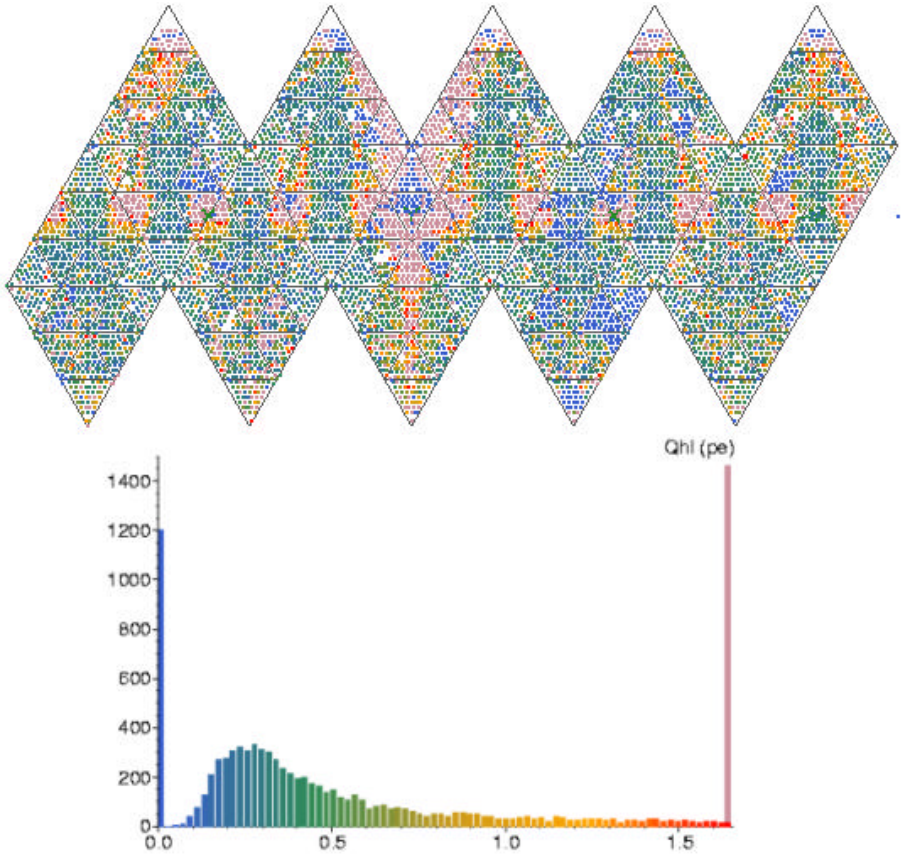

Figure 2.12: Reduced chi-squares for the PMTs with systematics folded into the error. PMTs that require high-angle laserball data for proper optical calibration appear to require even additional systematic uncertainty to be described as having a normally distributed efficiency about the mean. Below 1 reduced chi-square distribution indicates systematic and statistical error are correlated.

chi-square. PMT efficiency is not always normally distributed about a nominal value. A hypothesis that can made at this step is that the efficiency calculation, the measure of PMT efficiency, is inconsistent from one run to the next, and that the QE is not simply a number for each PMT. It is not unreasonable to posit that there is perhaps more information beyond the standard optics of the model fits included in the efficiency. It will be shown that this is indeed the case, in particular the PMTs that have significant and quantifiable variations in response at higher angles of incidence with respect to the PMT normal.

3. EFFICIENCY VARIATIONS INSIDE A SCAN

3.1 Local Spatial Variations

Two quantities of interest are the shape of the efficiency distribution and the 3-space distribution of efficiencies.

To construct the shape of the efficiency distribution, the fitted efficiencies from each PMT are first divided by the average fitted efficiency for that run. The bin corresponding to this number in a histogram is then incremented by one for each PMT. Finally the histogram is normalized to 10 000 (PMTs). This yields the fitted efficiency distribution about the mean as seen in figure.3.1. The efficiency distribution is close to Gaussian, as a simple Gaussian fit displays in its chi-square per degree of freedom value of 2.5.

To track down local spatial variations, the fitted efficiency data were plotted in a polar representation, the Z-direction polar angle going from 0 to 180 degrees, 0 being the top of the detector, and the azimuthal angle as measured from the x-axis going from -180 to 180 degrees as seen in figure.3.2. Azimuthal angle as measured from the x-axis is often refered to as X-Y plane polar angle in figures. From this representation low or high fitted efficiency "patches" of the detector can be seen. It appears as though the top portion of the detector has lower fitted efficiency than the lower portion, an up-down asymmetry. If one looks closely it seems as well that the PMTs in and around the belly plates appear to calibrate with very slightly higher fitted efficiency compared to the lower portion

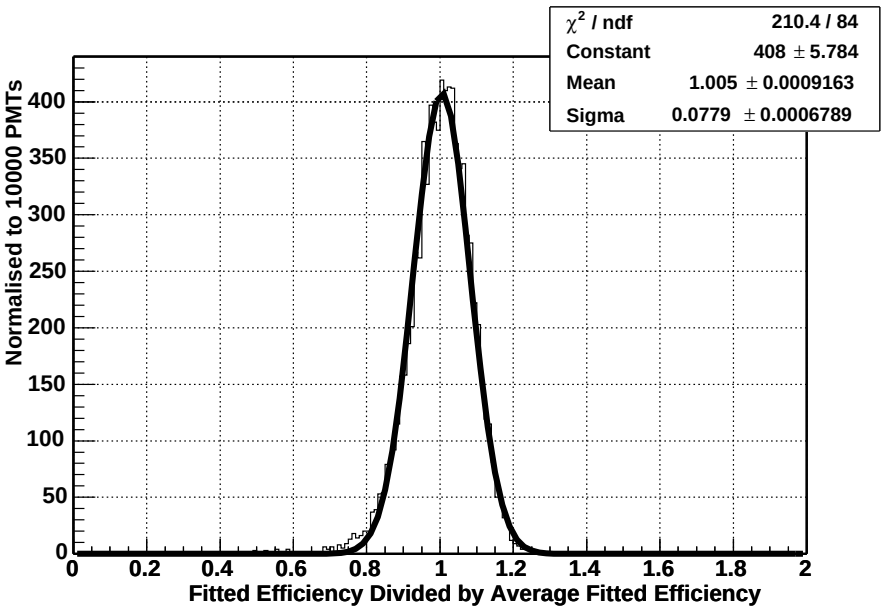

Figure 3.1: Fitted efficiency distribution for May 2002 at 420nm

of the detector. The projection and averaging of this fitted efficiency data along the polar angles confirm these visual conclusions (figure.3.3, figure.3.4). The average fitted efficiency at 90 degrees of azimuthal angle appears to be erratic. This is the position of the D_2O recirculation pipes. To obtain an efficiency in this region of the detector it requires very high angle off-center calibrations.

3.2 Variations Across Wavelengths

The fitted efficiency distribution at one wavelength can be compared one to a fitted efficiency distribution at another wavelength by simple overlay. These distributions are then fit to a Gaussian and the sigmas are tabulated in table.3.1. 620 nm is near the tail end of the PMT response and is thus quite broad. September 00 at 337 nm clearly has a skewed distribution. This is beleived to be as a result of fluorescence in the optical fiber leading to the laserball at that

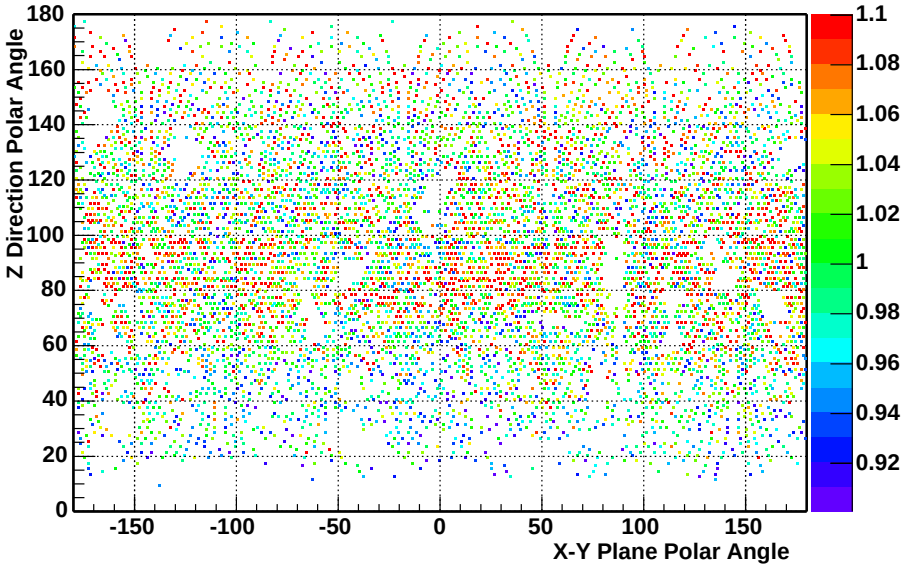

Figure 3.2: Polar display of fitted efficiencies for May 2002 at 420nm

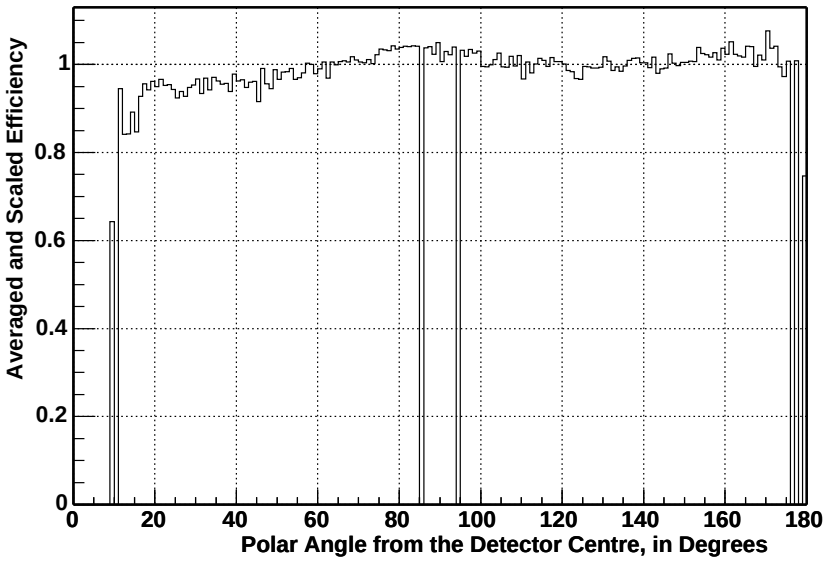

Figure 3.3: Up-Down asymmetry of fitted efficiency for May 2002 at 420nm

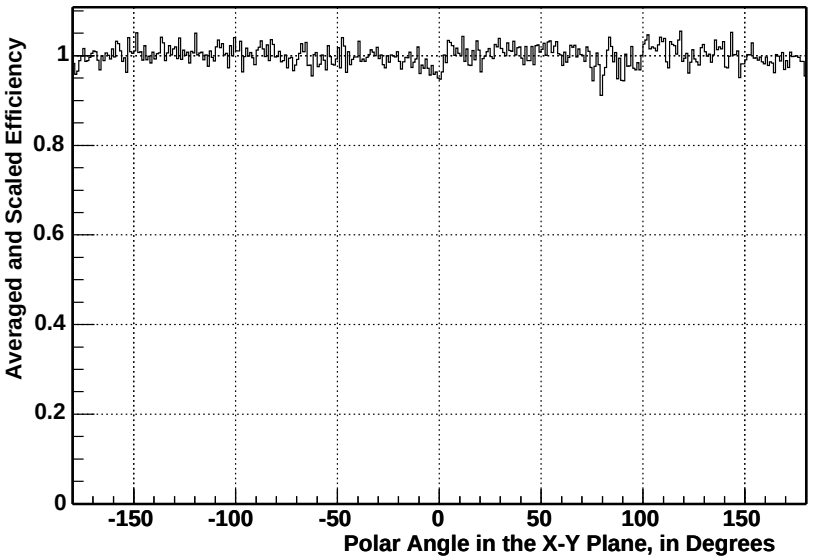

Figure 3.4: No azimuthal asymmetry of fitted efficiencies for May 2002 at 420nm

wavelength. The problem was discovered after the September 2000 scan and the fiber optic was replaced.

To compare a PMT's fitted efficiency from one wavelength to the same PMT's fitted efficiency at another wavelength the two quantities are each divided by the average fitted efficiency at the respective wavelength. The fitted efficiencies show strong correlations to all other wavelengths save those involving 620 nm (figure.3.8, figure.3.9, figure.3.10). The fitted efficiencies at 620 nm appear to be qualitatively different than other wavelengths. 500 nm fitted efficiency is better correlated with 620 nm fitted efficiency than the other wavelengths. The reasons behind this behavior are not understood. In his thesis B.Moffat [1] tabulates the measured attenuation coefficients (the αs from the optical model) in D_2O and H_2O. The attenuation coefficient for H_2O is significantly higher for 620 nm light, $(260 \pm 12)\ 10^{-5}\ cm^{-1}$, than the next highest attenuation length, $(56 \pm 16)\ 10^{-5}\ cm^{-1}$, for 337 nm light. The optical model should in principle

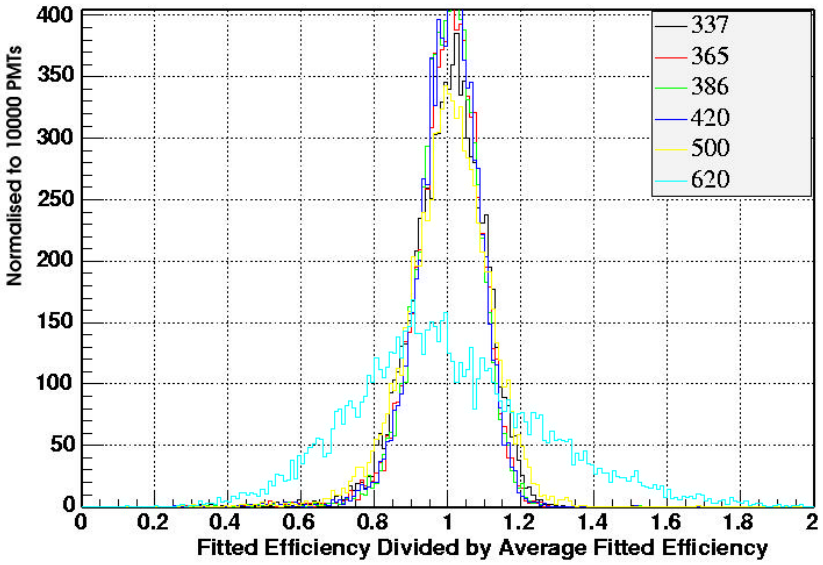

Figure 3.5: Overlay of the fitted efficiency distributions for May 2002

	Sigmas		
	May 2002	September 2001	September 2000
337 nm	0.0915 ± 0.0007	0.0925 ± 0.0007	0.1216 ± 0.0012
365 nm	0.0779 ± 0.0006	0.0802 ± 0.0007	0.0813 ± 0.0007
386 nm	0.0780 ± 0.0007	0.0786 ± 0.0007	0.0791 ± 0.0007
420 nm	0.0778 ± 0.0006	0.0785 ± 0.0007	0.0779 ± 0.0007
500 nm	0.1039 ± 0.0009	0.1042 ± 0.0009	0.1023 ± 0.0009
620 nm	0.2451 ± 0.0023	0.2565 ± 0.0023	0.2613 ± 0.0022

Table 3.1: Sigmas and errors of Gaussian fits to fitted efficiency distributions

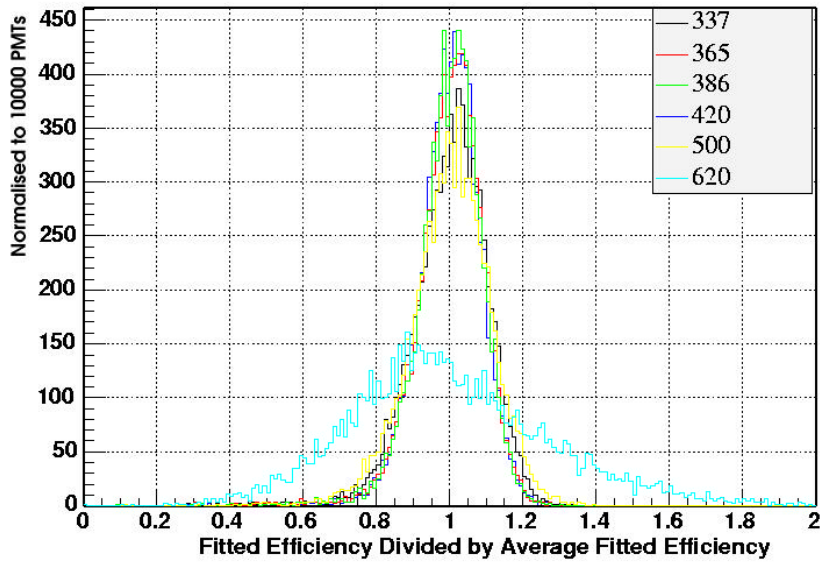

Figure 3.6: Overlay of the fitted efficiency distributions for September 2001

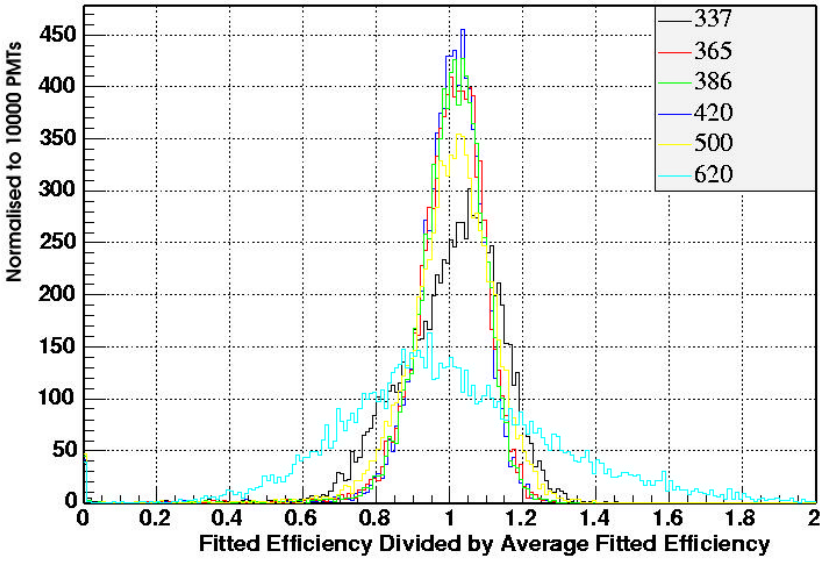

Figure 3.7: Overlay of the fitted efficiency distributions for September 2000

take this effect fully into account. There may be reason to believe that the path difference in prompt light between directly incident light on the PMT and light that first impacts a reflector and is then reflected into the PMT may be sufficient to account for this behavior. Another possible explanation may come from the fact that the PMTs were constructed for optimal efficiency at 420 nm. At 620 nm, in the tail end of the efficiency curve, individual PMT characteristics may be more disparate. However as of writing this thesis both ideas remain speculation.

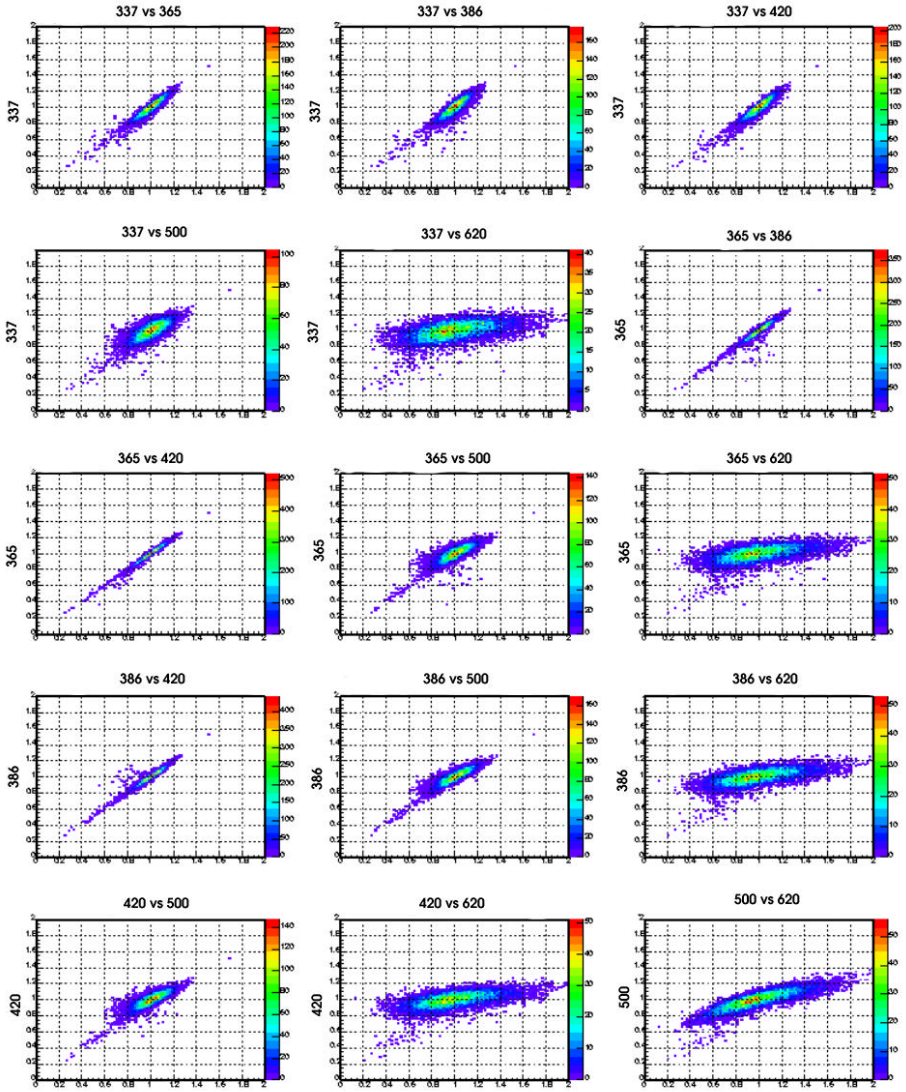

Figure 3.8: Correlations between fitted efficiency at all wavelengths in May 2002. 620 nm is qualitatively different than the other wavelengths, possibly due to the relatively high opacity of H_2O at this wavelength compared to the others.

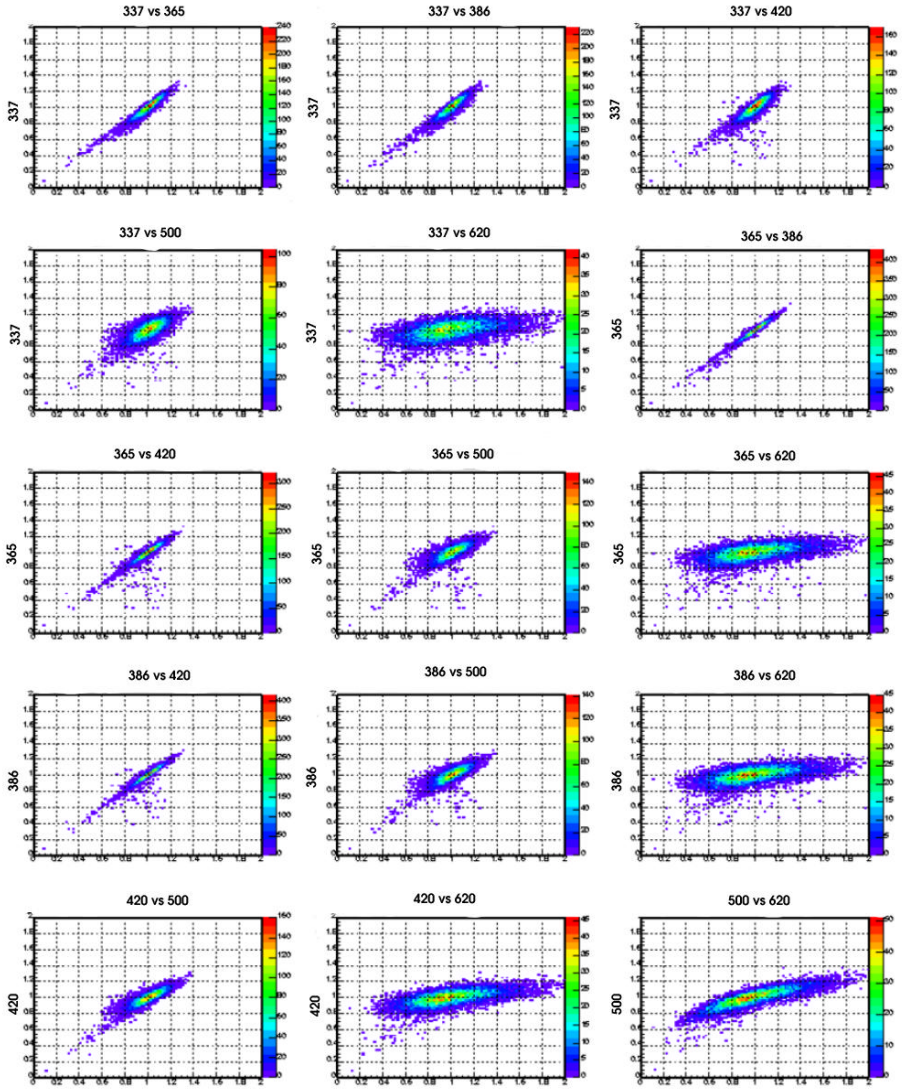

Figure 3.9: Correlations between fitted efficiency at all wavelengths in September 2001

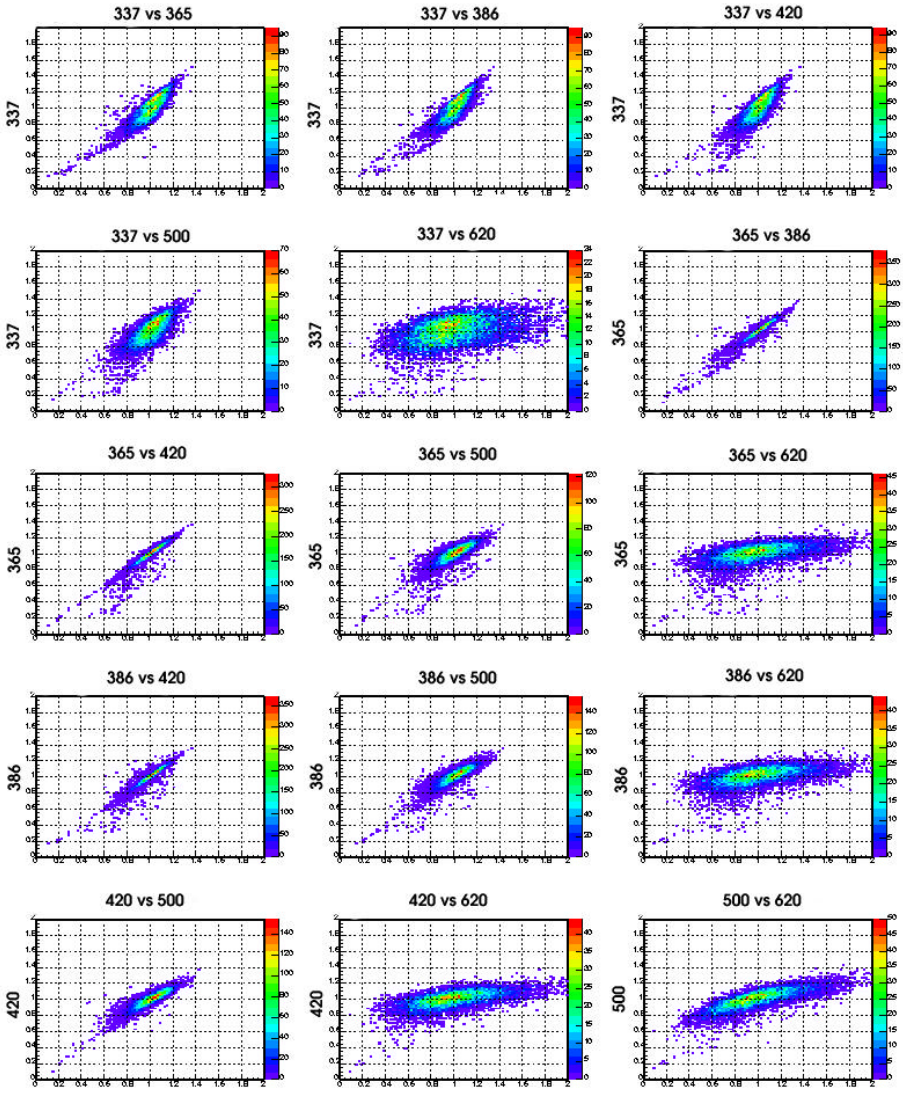

Figure 3.10: Correlations between fitted efficiency at all wavelengths in September 2000

4. EFFICIENCY VARIATIONS ACROSS SCANS

A straightforward overlay comparison of all the optics data to date leads to some interesting global characteristics of the efficiencies. With a more detailed analysis the global characteristics can be further generalized to the statement of the stability of the relative efficiencies.

4.1 Global Efficiency Variations

As can be gleaned from table.3.1 the efficiency distributions are quite stable and the overlay can be seen in figure.4.1. The discrepancy between September 2000 and other scans at 337 nm is again attributed to a change in the laserball optical fiber used to conduct the light from the laser to the laserball. This fluorescence shifts some portion of the laser light into higher wavelengths and thus ruins the assumption of monochromatic light in the model fits. The up-down asymmetry in efficiency is a property of the detector over all wavelengths as well as the symmetry in the other polar angle, figure.4.2 and figure.4.3. The September 2000 azimuthal projection exhibits a dip in its profile at 90 degrees. This can be attributed to anomalously low efficiencies around a particular belly plate during this scan and can be readily seen in figure.4.4.

4.2 Individual PMT Efficiency Variations

To compare a PMT's fitted efficiency from one scan to the same PMT's fitted efficiency in another scan the two quantities are divided by the average fitted efficiency in their respective scan to obtain distributions centered about 1. This yields the variations in time of a given PMT's fitted efficiency relative to the average fitted efficiency of all PMTs.

The variation in time of a given PMT's fitted efficiency relative to the average fitted efficiency of all PMTs can be seen in figure.4.5.

Similar plots as the ones constructed to detect local efficiency variations inside a scan are constructed to investigate variations in time of PMT fitted efficiency relative to the average fitted efficiency of all PMTs. figure.4.6. is the polar representation, figure.4.7 is the Z-direction polar angle averaged representation and figure.4.8 is the azimuthal angle averaged representation.

Furthermore a correlation plot is constructed to verify that PMTs with above or below average fitted efficiency in a scan remain above or below average fitted efficiency in the following scan. This is true and can be seen in figure.4.9.

The complete set of figures then follows. There are sporadic variations in time of fitted efficiency across the detector, sometimes on the order of 20%, most notably for PMTs situated behind the recirculation pipes. These variations are however small compared to the global trend of stability. The up-down asymmetry detected earlier is not changing as the detector ages. PMTs with above or below average fitted efficiency in one scan remain above or below average fitted efficiency in another scan as seen in the correlation plots. The introduction of salt into the D_2O appears to have no effect on the efficiencies. This lends further confidence for the optical model.

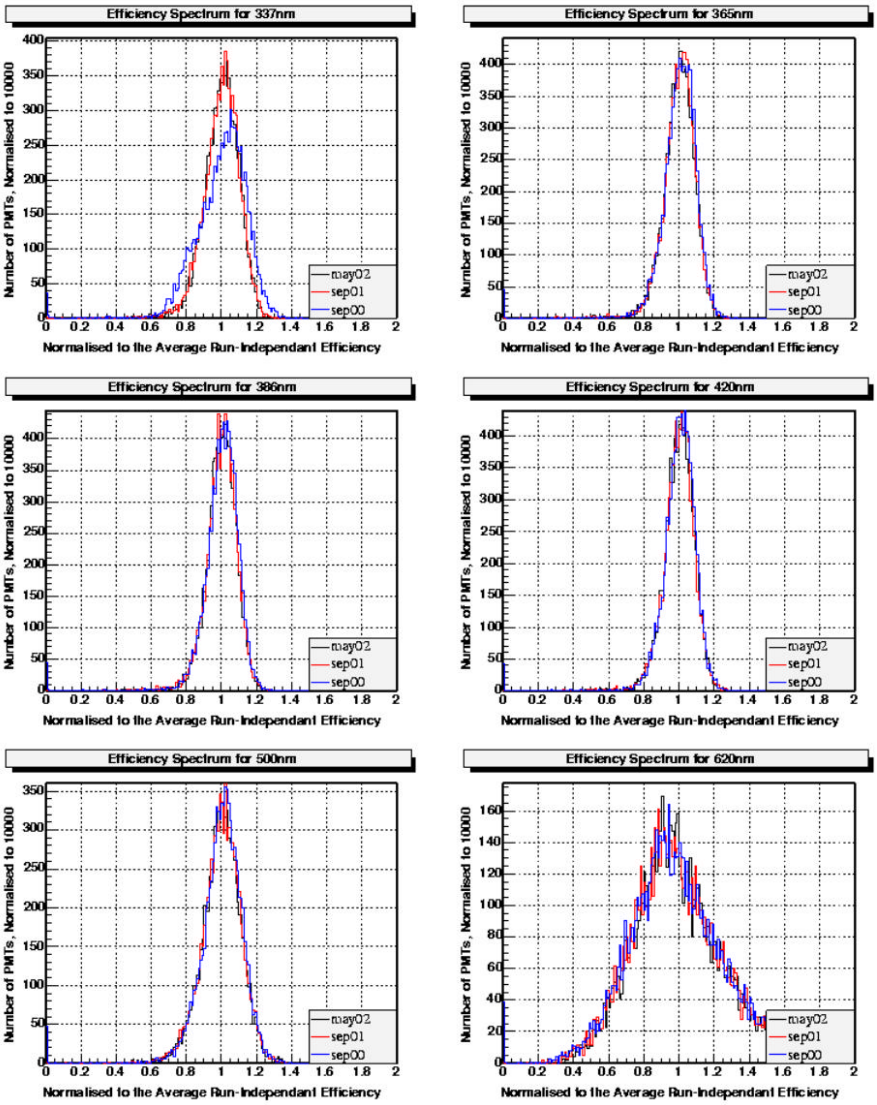

Figure 4.1: Fitted efficiency distributions, all scans, all wavelengths

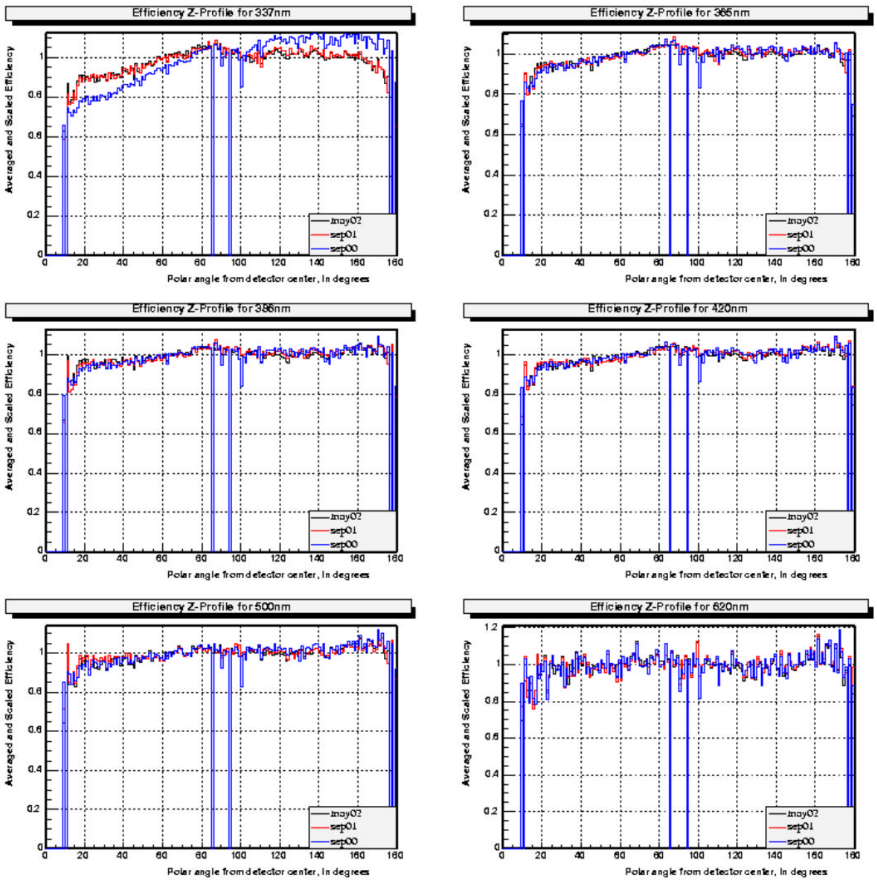

Figure 4.2: Up-Down Asymmetry, all scans, all wavelengths

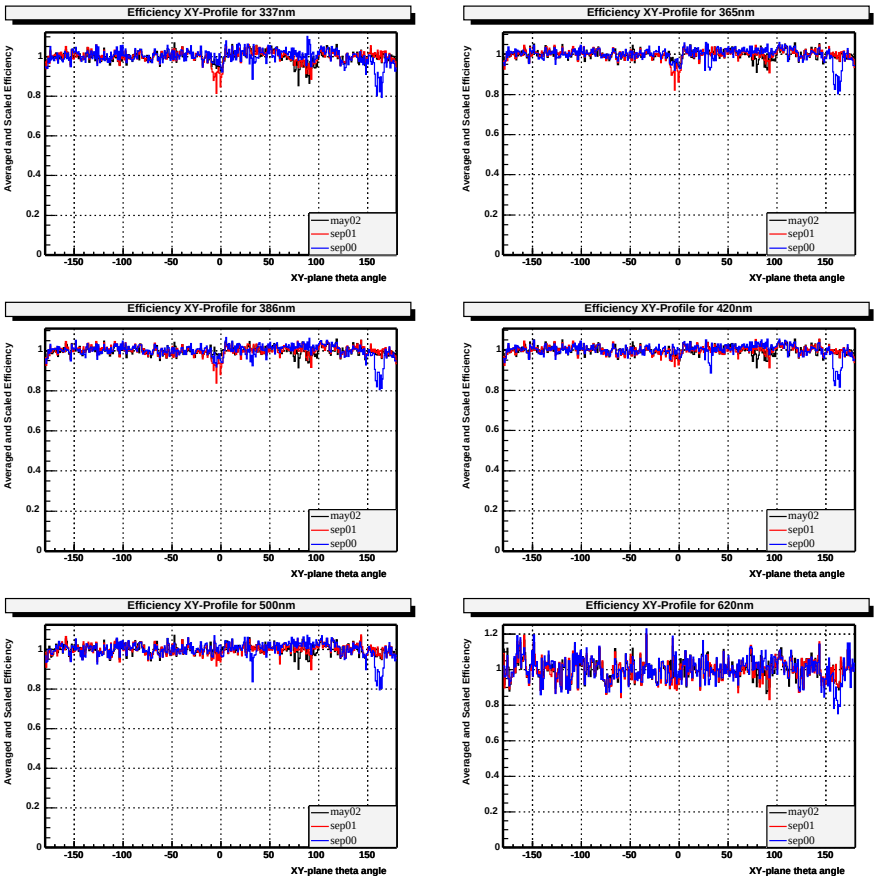

Figure 4.3: No XY-plane Polar Angle Asymmetry, all scans, all wavelengths

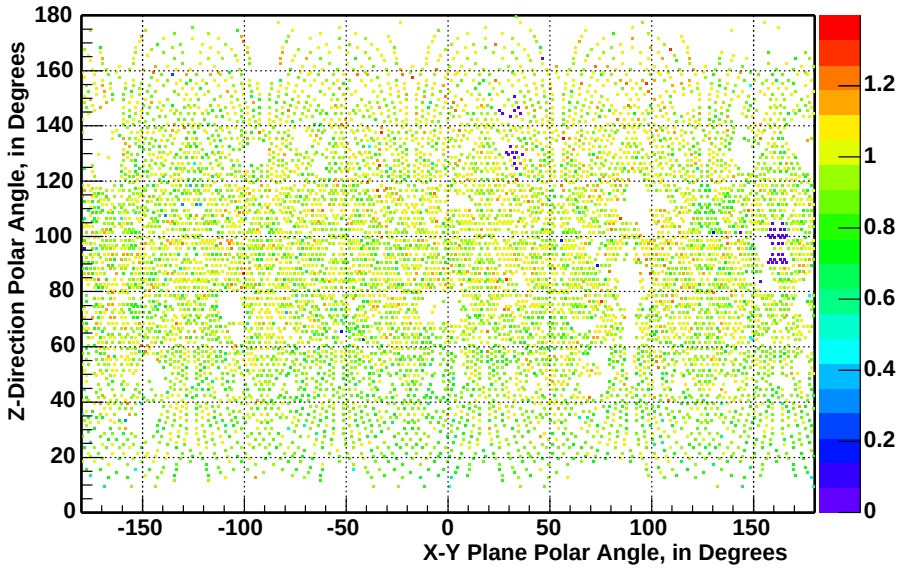

Figure 4.4: Display of September 2000 Low Efficiency Patch of PMTs at 160-170 degrees in purple

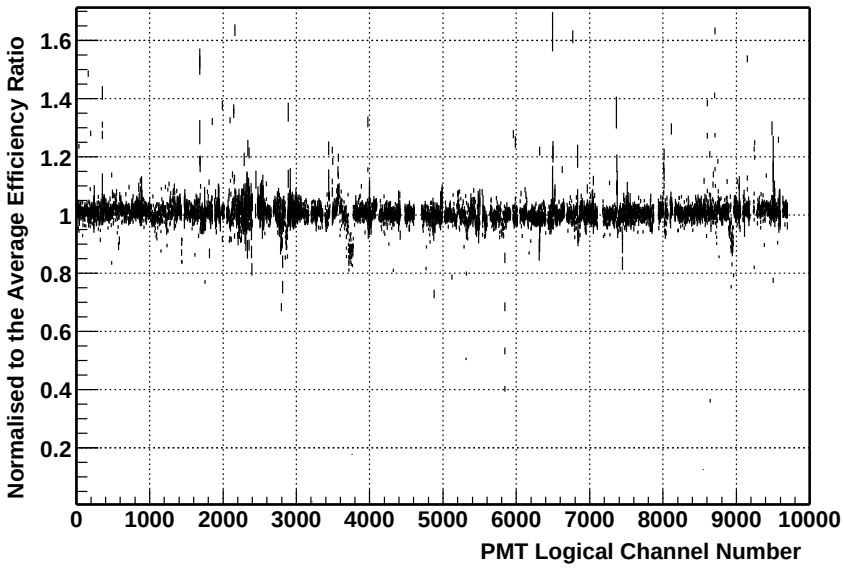

Figure 4.5: Ratio of September 2000 to September 2001 efficiencies at 420 nm

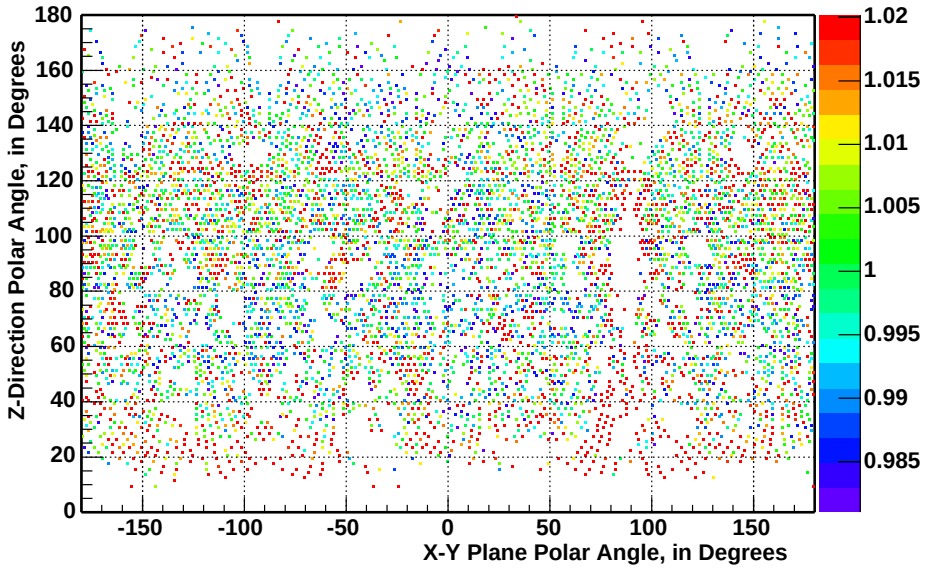

Figure 4.6: Polar representation of the variation in time of a PMT's fitted efficiency relative to the average fitted efficiency of all PMTs for September 2001 data to May 2002 data at 500 nm

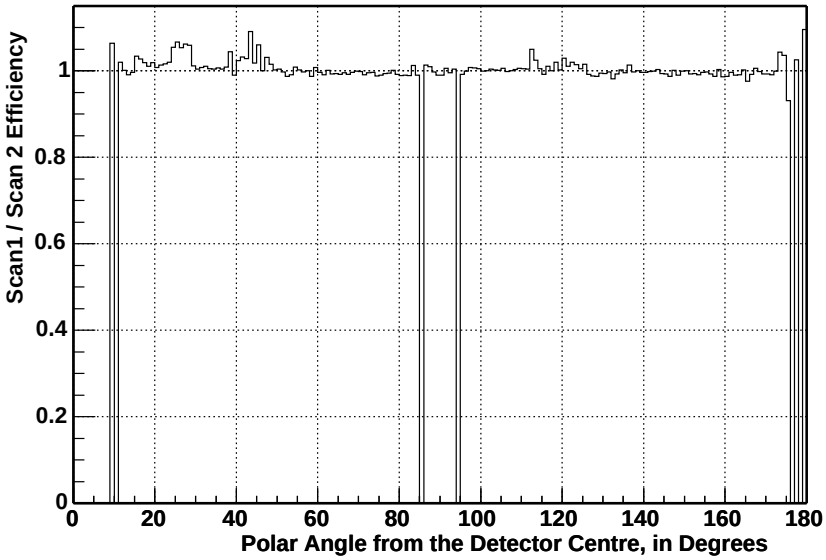

Figure 4.7: Z-direction polar angle representation of the average variation in time of PMT fitted efficiency relative to the average fitted efficiency of all PMTs for September 2001 data to May 2002 data at 500 nm

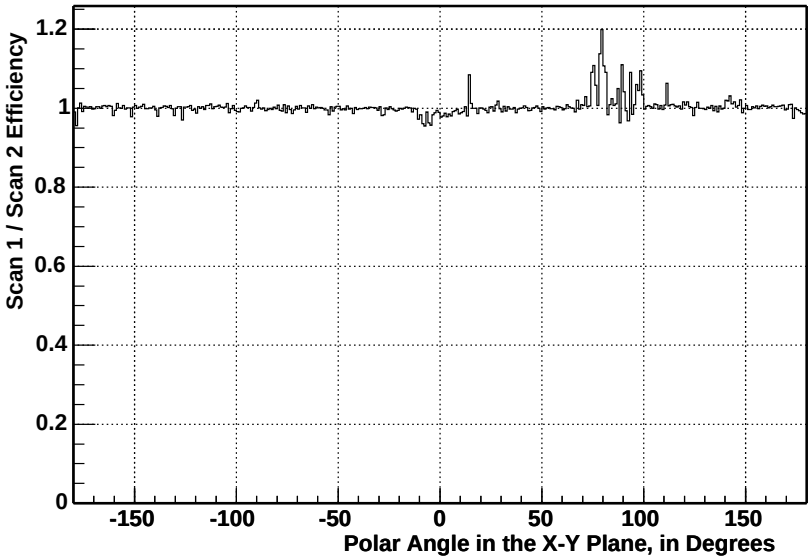

Figure 4.8: Azimuthal angle representation of the average variation in time of PMT fitted efficiency relative to the average fitted efficiency of all PMTs for September 2001 data to May 2002 data at 500 nm

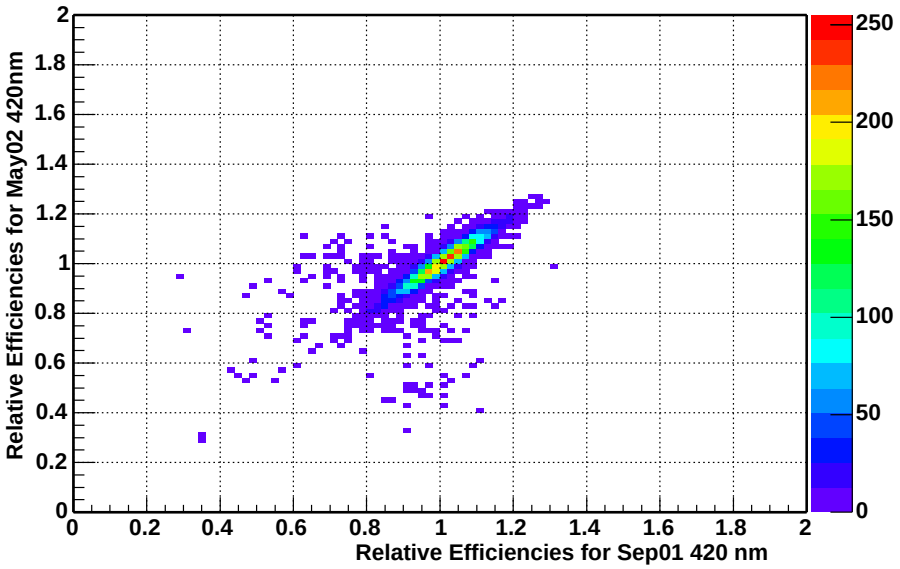

Figure 4.9: Correlation between May 2002 fitted efficiencies to September 2001 fitted efficiencies for each PMT at 420 nm, relative to their respective average fitted efficiency

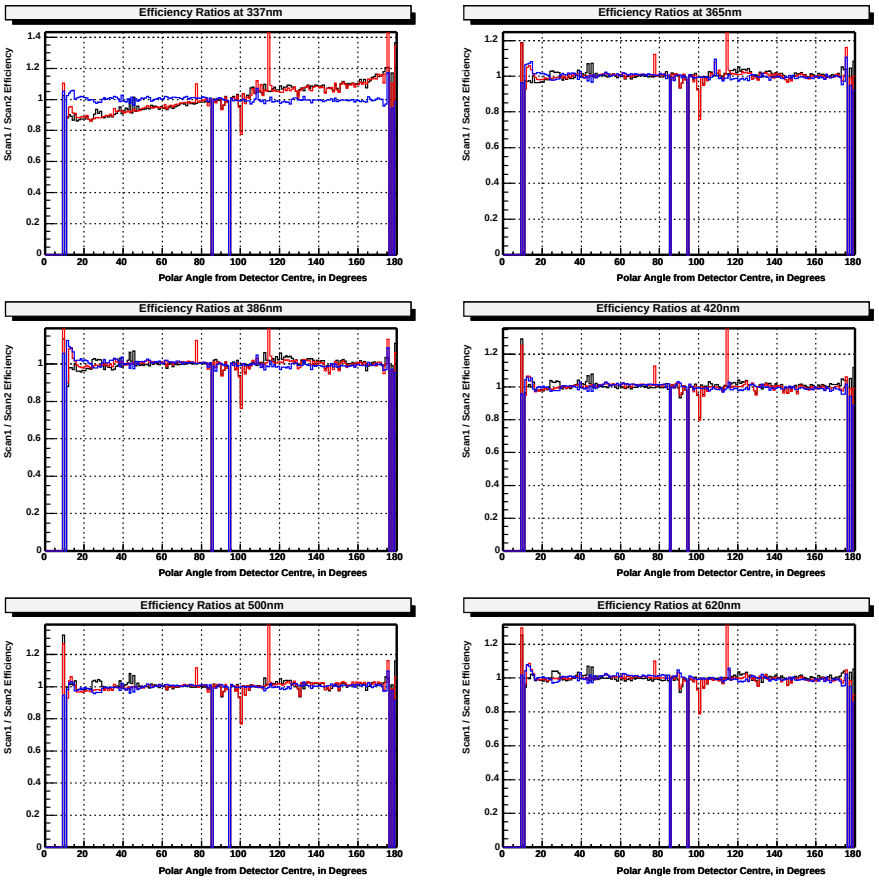

Figure 4.10: The up-down asymmetry in fitted efficiency remains the same through time. September 2000 at 337 nm is skewed perhaps because of fiber-optic fluorescence.

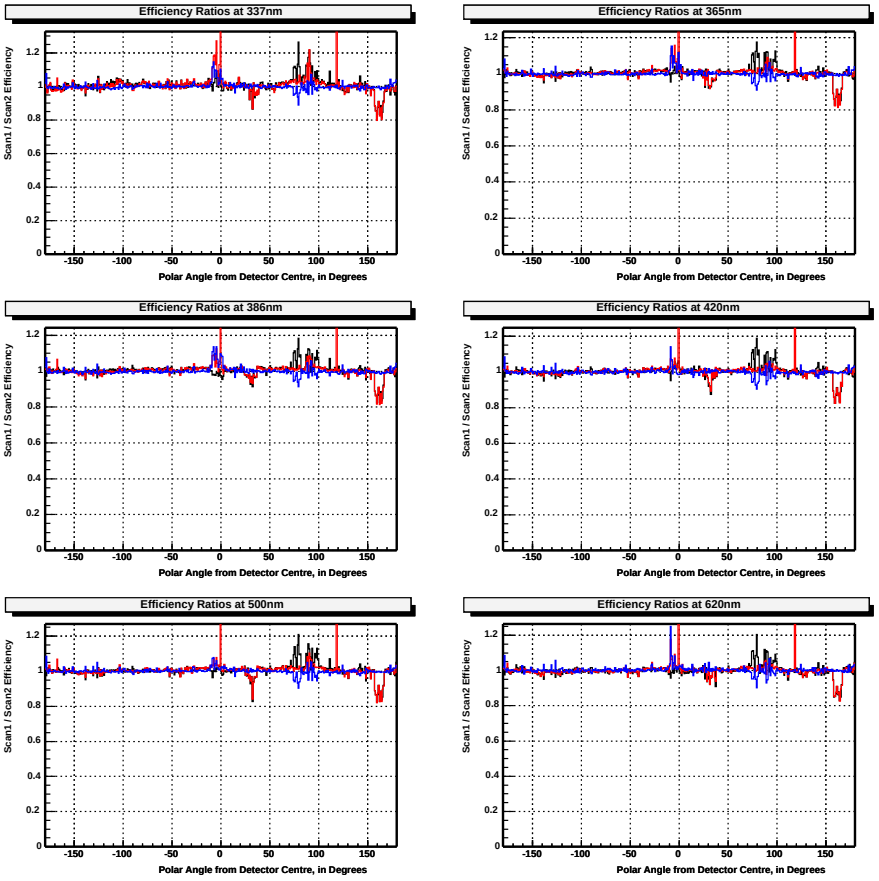

Figure 4.11: Fitted efficiency remains stable across azimuthal angle. The PMTs situated behind the D_2O recirculation pipes are situated at 90 degrees and appear to vary significantly over time, a likely consequence of the optical difficulties in calibrating these PMTs.

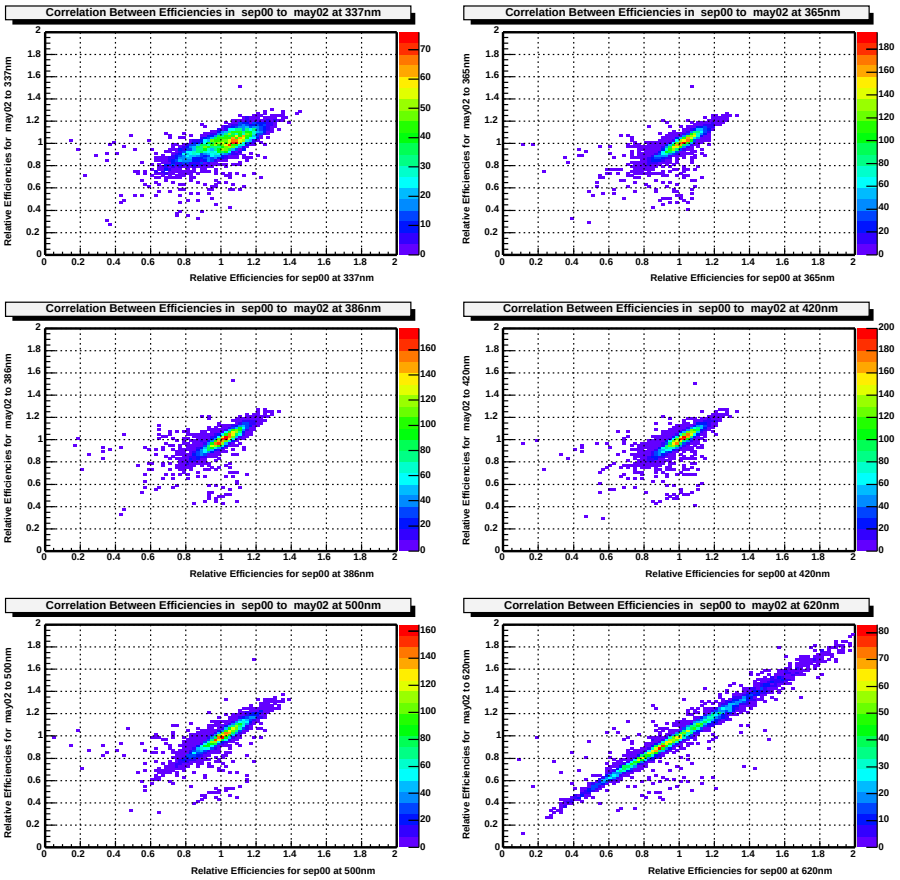

Figure 4.12: Fitted efficiency correlations May02 to Sep01. 620 nm fitted efficiency spread perhaps correlates with the path length through light water

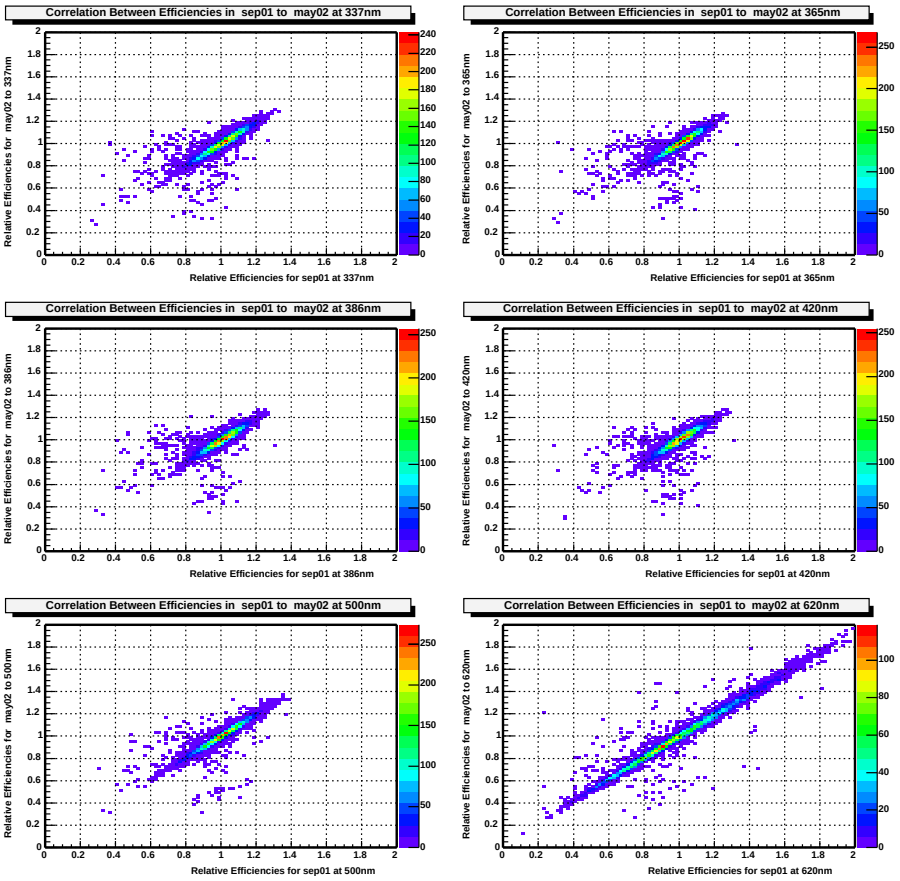

Figure 4.13: Fitted efficiency correlations May02 to Sep00

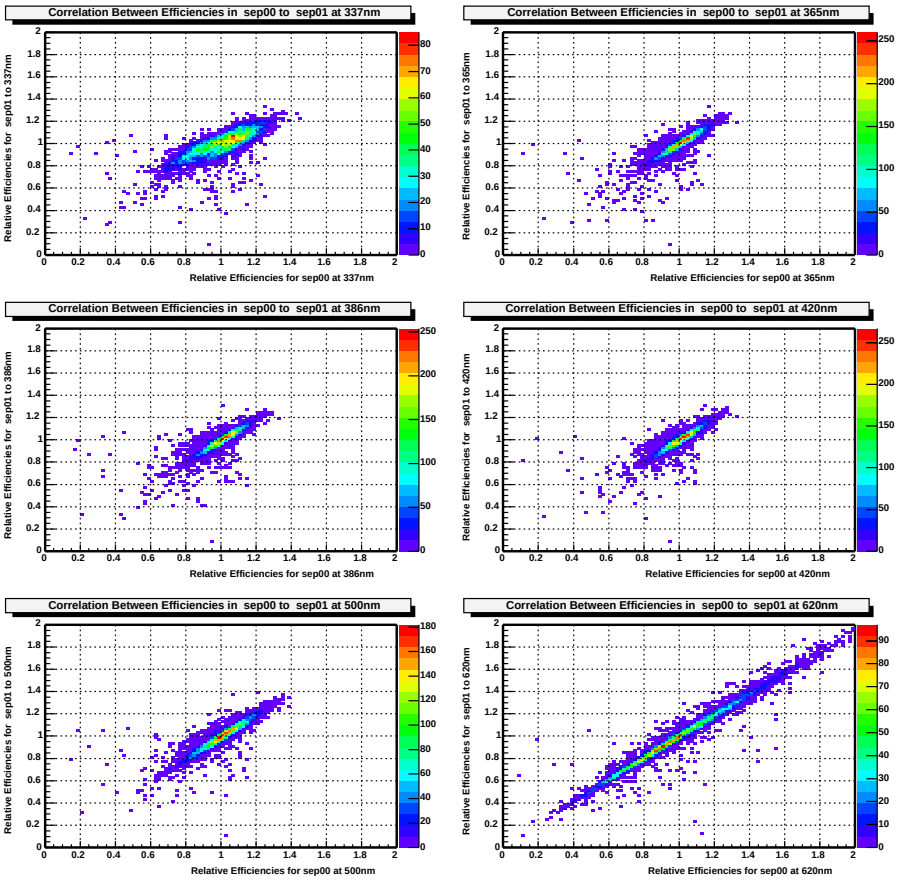

Figure 4.14: Fitted efficiency correlations Sep00 to Sep01

5. EFFECTS OF INCIDENCE ANGLE ON EFFICIENCY

In B.Moffat's conclusion to his thesis he mentioned how much he would have enjoyed to clearly characterize the PMT response at higher incidence angles that he was only able to glimpse at with his limited dataset and limited time. In Chapter 1. the efficiency is shown to be less than completely described by statistics and the 8 systematics tested. These facts combined demand that PMT efficiency as a function of incidence angle be investigated.

5.1 Greater Variability at Higher Incidence Angles

What B.Moffat saw in his analysis was that as the laserball light's incidence angle increased relative to the PMT normal, the PMT efficiency distribution got significantly broader, by a factor of about 1.8. This is seen in this analysis as well. A two-dimensional histogram figure.5.1, binned in efficiency and incidence angle, is incremented by one for each efficiency measurement made at that angle of incidence divided by the fitted efficiency for the particular PMT. Dividing by the fitted efficiency for the PMT removes PMT to PMT differences in fitted efficiency. The distribution of efficiencies centered about the fitted efficiency is thus obtained.

The distribution of efficiencies about the fitted efficiency along the angle of incidence yields the global efficiency variability at that angle. The global efficiency variability at a given angle is then fit to a Gaussian and the sigma

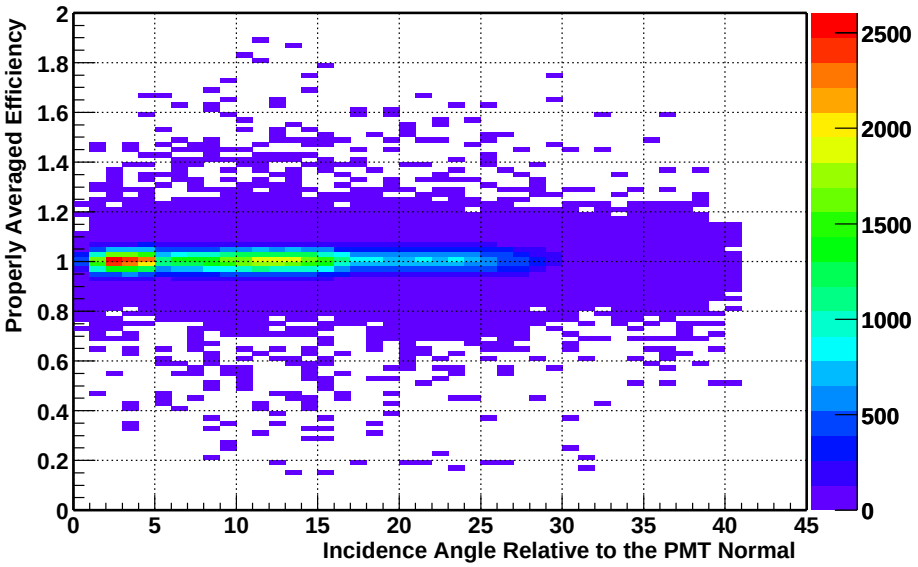

Figure 5.1: PMT efficiency distribution as a function of the angle of incidence, May02 at 420nm

values of the fit quantify the efficiency angular variability figure.5.3 .

The efficiency angular variability is then tabulated for all angles in a histogram that clearly shows the same behavior B.Moffat noted in his thesis figure.5.2. At the very highest angles there is very little data and the fits are poor, creating

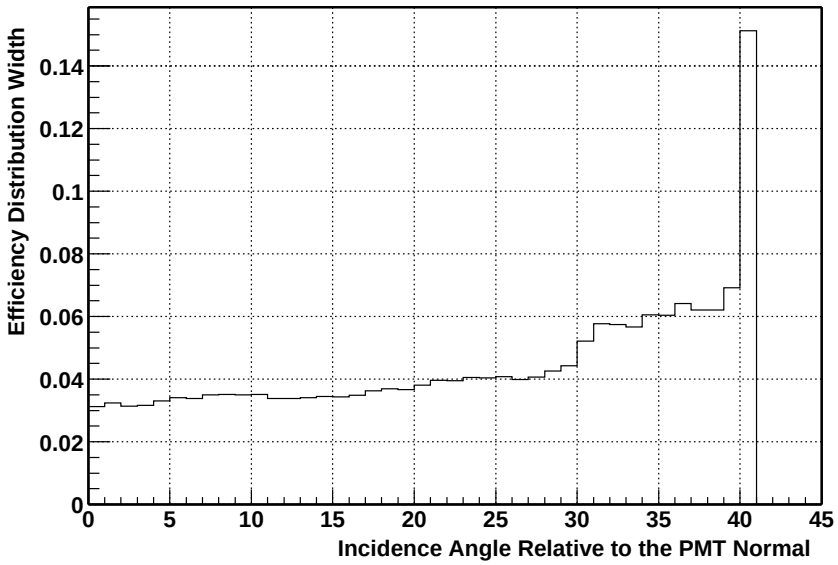

Figure 5.2: PMT efficiency distribution broadening about the fitted efficiency for May02 at 420nm

a large spike at the end. This high angle spike is an artifact of the fit and not physical. For a typical wavelength and scan the number of efficiencies taken at 30 degrees angle of incidence is on the order of a thousand. At the most extreme angles of incidence there can be fewer than a hundred PMTs and the Gaussian is very choppy and largely flat which engenders wild values of sigma from the Gaussian fit.

The angular variability is seen in all scans at all wavelengths, figure.5.4. Some scans do not have data at comparable high angles to others. This is simply a question of how much time the calibration team had to do the scan

and potential source manipulator system issues. To get the highest angle data the laserball source needs to be brought very close to the acrylic vessel and this is not always achieved for a variety of technical reasons (not the least of which is the detector schedule).

5.2 Explanation of Efficiency Variability

Two schemes can be envisioned to explain this global efficiency variability at higher angles of incidence. In the first scheme each PMT is different: one PMT gradually edges up in efficiency as the angle increases and yet another gradually drops in efficiency. A second potential scheme is that all PMTs are the same: It is simply a matter of the measurement at high angles being less well defined - for instance a significant variation in the plane-polar "ϕ" angle between the internal elements of the PMT and the external light source. In this section the second scheme is validated.

First a visual inspection method was performed. A large number of plots of efficiency vs. incidence angle for individual PMTs were generated to look for any clear trends. It was not obvious from this initial investigation of the data that the first scheme would turn out to be true.

The correlation plot figure.5.6 of the 30 degree efficiency vs the 1 degree efficiency demonstrates that there is no clear correlation between the efficiency at normal incidence and the efficiency at high angles. This was also observed at all other wavelengths in all scans.

As a cross check the 1 degree efficiency vs the 1 degree efficiency was plotted and shows perfect correlation (confirming no error in the otherwise very complicated code!).

Each PMT has an identical internal elements which are not symetric in ϕ, namely the plates are square. Each PMT was installed in the PSUP with a different orientation. The source of the variability may well turn out to be as a result of a ϕ dependance common to all PMTs. Time constraints prohibited investigation.

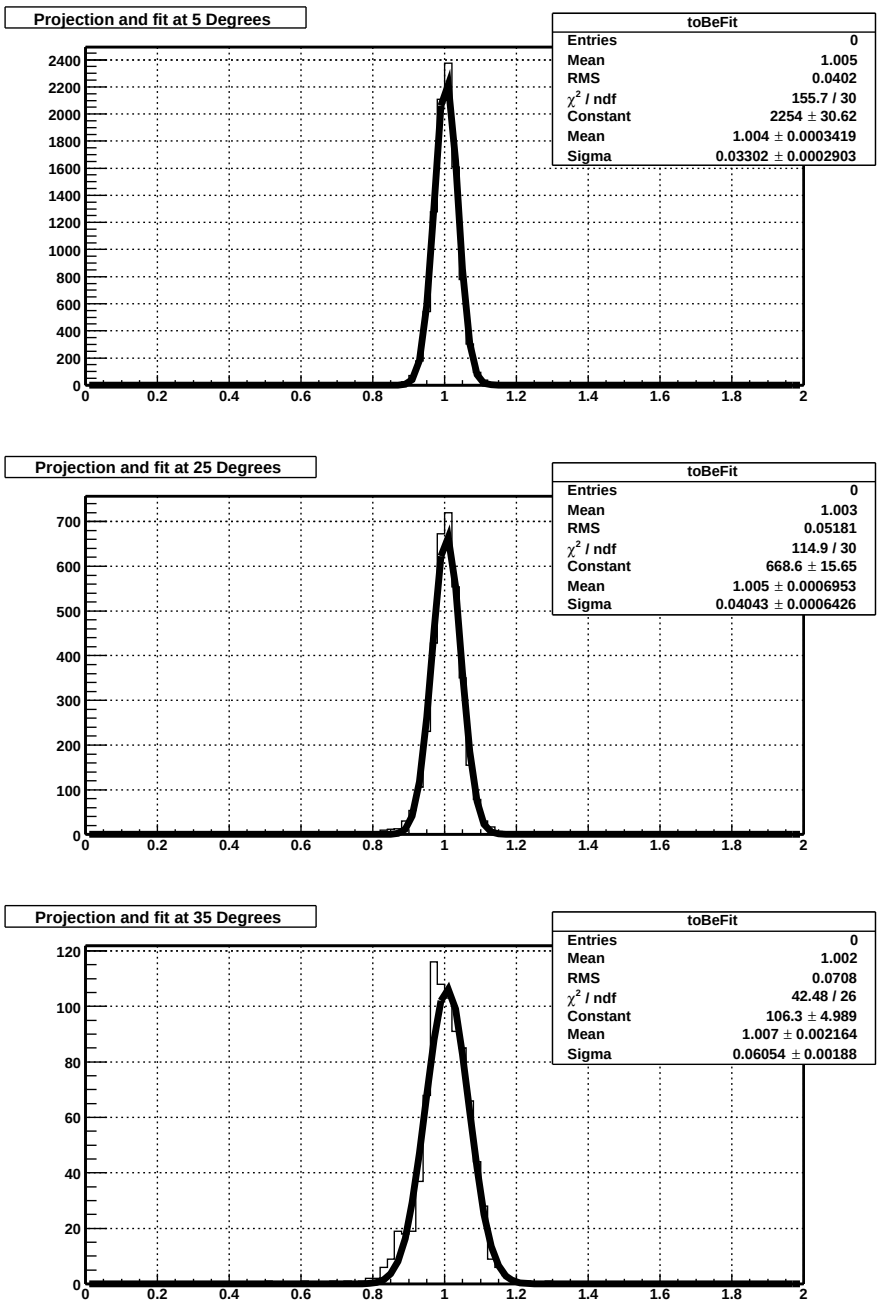

Figure 5.3: Sample efficiency distribution broadening about the fitted efficiency for May02 at 420nm. The width of the distribution (sigma) increased from 0.03 to 0.06 as incidence angle goes from 5 to 35 degrees

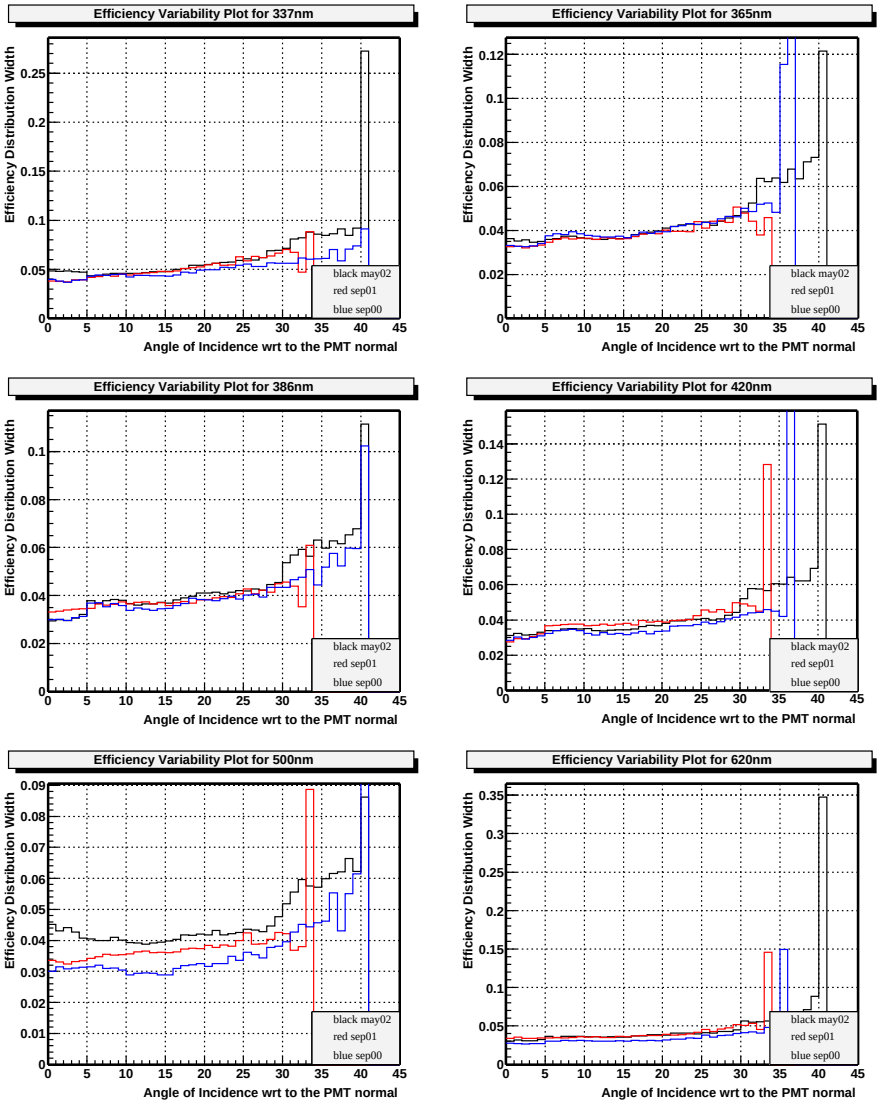

Figure 5.4: Greater efficiency variability at higher angles of incidence is seen at all wavelengths and for all scans

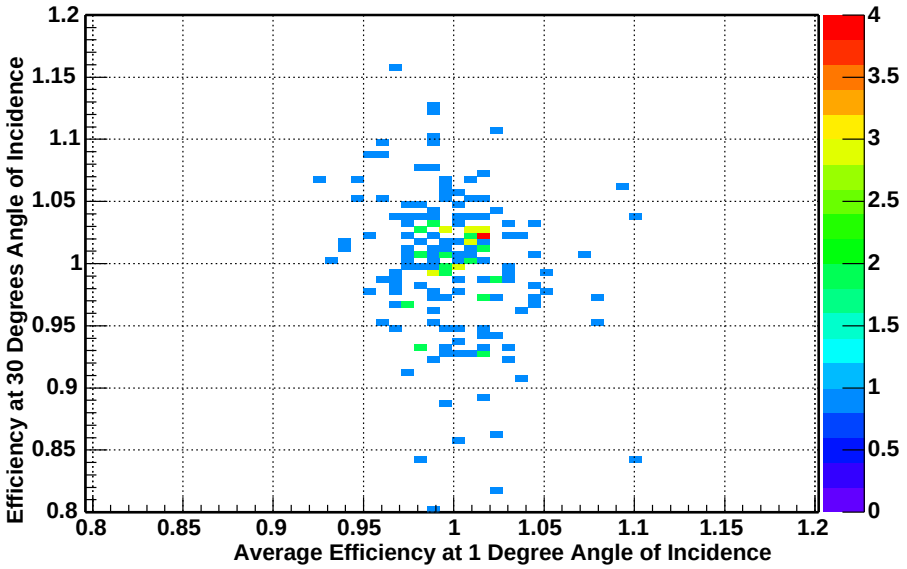

Figure 5.5: Correlation plot of all fitted efficiency measurements at 30 degrees angle of incidence vs. average fitted efficiency at 1 degree angle of incidence for May02 420nm

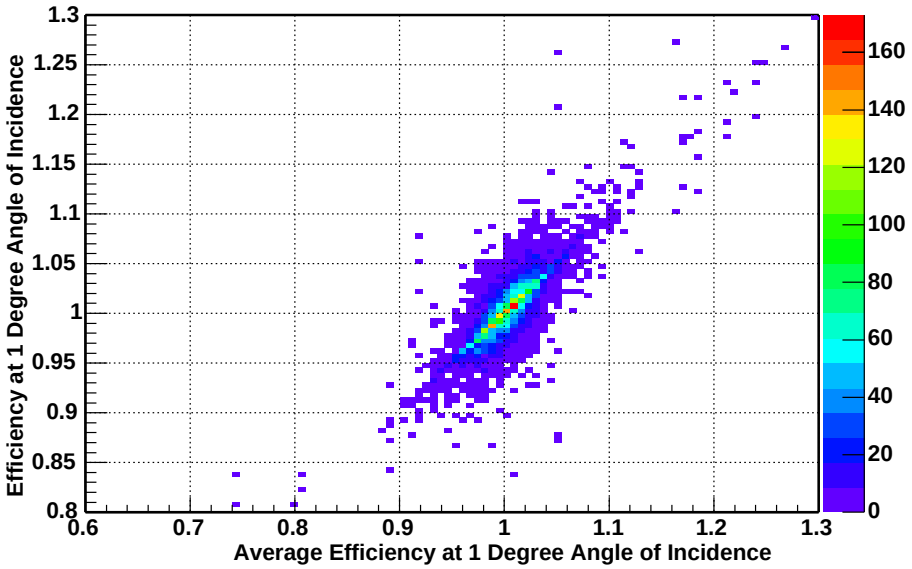

Figure 5.6: Correlation plot of all fitted efficiency measurements at 1 degree angle of incidence vs. average fitted efficiency at 1 degree angle of incidence for May02 420 nm

6. CROSS CHECKS

This chapter deals with the various cross-checks employed to give confidence to the results of this thesis.

6.1 PMT Attribution

With so many PMTs, global characteristics can easily overshadow discrepancies at the individual PMT level. Tube numbering, inferring the correct efficiency from the correct tube, is of critical importance. XSnoed is a program developed by Phil Harvey [5] to visualize SNO data. The PMT numbering scheme used in this thesis, LCN, is also the numbering scheme that the XSnoed viewer interprets data. If a histogram of 10000 bins is fed to XSnoed, the program will associate the information in bin 0 with the tube of LCN 0 and display the information in the 3D model of the detector. This is how certain graphical data displays were generated in this document. A simple visual cross-check that the data is being correctly assigned is to look at the features of the detector in XSnoed. Figure.2.6 clearly displays the belly plates and finer structure - the support ropes.

6.2 PMT Accounting

Not every PMT has a fitted efficiency and it is important to understand why this is. For a PMT to have a fitted efficiency in a given scan at a given wavelength it requires only a single efficiency from a single run in that scan at that wavelength. The cuts applied to the data are as follows:

- Occupancy
- fBad - a label used to distinguish PMTs with optical calibration difficulties

A PMT in a given run has no efficiency if it has no occupancy. For a given run, the laserball position may not be in a position where optical difficulties can be easily accounted for, the PMT then has an fBad label of 11 or 1, and even if it has occupancy for that run it is cut. The data cuts are completely understood and accounted for as can be seen in table.6.2.

The principal reasons a PMT does not have an efficiency in a given run are:

- DQXX - permanently turned off PMTs (DQXX banks)
- CHCS - "misbehaving" or malfunctioning PMTs (CHCS banks)
- fBad
- Rch time-profile

A PMT or the electronics associated with a PMT can occasionally breakdown. These breakdowns often cause undesirable effects on the data collected from other, functional, PMTs and electronics. The offending PMTs are then turned off until maintenance can be performed. Most electronics related problems are readily fixed and the PMT will be put back into service after maintenance. If a problem originates from the PMT then it cannot be readily repaired and then these PMTs are permanently turned off. For any given run the information of which PMTs are turned off is stored in the DQXX banks. One

	PMTs with				
	fitted efficiency	no fitted efficiency	always no occupancy	always fBad 1 or 11	occupancy only when fBad 1 or 11
May 02					
337 nm	8172	1281	1166	102	13
365 nm	8176	1277	1166	100	11
387 nm	8176	1277	1166	100	11
420 nm	8176	1277	1166	100	11
500 nm	8177	1276	1166	99	11
620 nm	8173	1280	1166	101	13
Sep 01					
337 nm	8271	1182	1014	167	1
365 nm	8273	1180	1014	165	1
386 nm	8273	1180	1014	165	1
420 nm	8271	1182	1014	167	1
500 nm	8273	1180	1014	165	1
620 nm	8271	1182	1014	167	1
Sep 00					
337 nm	8515	938	784	153	1
365 nm	8552	901	755	139	7
386 nm	8514	939	785	153	1
420 nm	8547	906	758	140	8
500 nm	8511	942	786	153	3
620 nm	8500	953	765	186	2

Table 6.1: Detailed accounting of the cuts that lead to the number of PMTs with no fitted efficiency across all wavelengths and scans

important and simple cross-check is to verify that these PMTs with no applied voltage have no fitted efficiency. Because the data span multiple runs, there was the possibility that the individual runs would have different PMTs turned off in DQXX. Analysis of the DQXX files shows that the data runs in the May 2002 scan all have the exact same PMTs turned off and these PMTs have no fitted efficiency. The data runs in September 2001 scans as well all have the exact same PMTs turned off, and these PMTs have no fitted efficiency. In the September 2000 scan 104 runs have the exact same number of PMTs turned off. There were 17 runs in September 2000 which have additional PMTs turned off in a single crate beyond those turned off in the 104 other runs. PMTs turned off common to all 121 runs have no fitted efficiency.

Another important bank, CHCS, contains the information on which PMTs are "misbehaving" but are not turned off because they have not (at the time) caused problems to the data as a whole. This bank is created for a spread of runs, not for an individual run. The September 2000 and September 2001 data sets are each accounted for by a single CHCS table. The May 2002 dataset spans two CHCS tables but these tables are found to be identical. Not all PMTs described in CHCS have no fitted efficiency. However many PMTs without fitted efficiency are found in CHCS.

Taking the three components, DQXX, PMTs that always have fBad 1 or 11, and CHCS together does not account for all PMTs without fitted efficiencies as can be seen in table.6.2. The remaining PMTs which have no fitted efficiencies are all PMTs which have zero occupancy. Some effort is made here to track down the reasons behind why these remaining PMTs have no occupancy, but this quickly falls beyond the scope of this thesis.

The OCA data trees are developed from Rdt and Rch files. The occupancy of a PMT in an OCA-tree is proportional to that PMT's Rch time integral and to that PMT's Rdt counts. If a PMT's Rch time integral is zero then it has no occupancy. Some of the PMTs which are not accounted for by DQXX,

CHCS, and fBad always have a zero Rch-time integral. These PMTs are thus "legitimately" off. Similar to the occupancy cuts, some PMTs have non-zero Rch time integral only during runs where the PMT is fBad 1 or 11. There is a one-to-one correspondence between the PMTs with occupancy only when fBad equals 1 or 11 and the PMTs with an Rch time integral only when fBad equals 1 or 11. There remain PMTs which have an Rch time integral which upon inspection appears to be normal, and furthermore register a positive Rdt-counts value, but do not posses an occupancy at the OCA tree level. The only salient characteristic that has been determined to date is that these remaining PMTs are all the same across wavelengths inside a scan and are largely distributed along specific cards.

6.3 Thresholds, Voltage, Crates and Channels

Another influence on efficiency is threshold. Threshold is an electronic cut-off in which pulses from the PMT that do not reach a certain voltage threshold are ignored. This is set primarily to offset electronic "noise", or misfires, which do not correspond to the PMT actually detecting a photon. However by setting a threshold some weak signal photon detections are lost as well in the process. PMTs with lower threshold should produce correspondingly more pulses and by the definition of QE they should have higher efficiency. Threshold is set according to the electronic channel number and ranges in an arbitrary scale from 0 to 255.

There is a correlation between threshold and fitted efficiency. This can be readily seen by eye in the profiles of average threshold and average efficiency binned according to electronic channel number in figure.6.2 and figure.6.3. The fitted efficiencies were compared to thresholds for all wavelengths and across all scans and the correlation is clearly visible in figure.6.4, figure.6.5 and figure.6.6. PMTs with higher threshold have lower fitted efficiency as expected, figure.6.7.

	PMTs with no fitted efficiency						
	total	turned off in DQXX	flagged problem-atic in CHCS	always fBad 1 or 11	and zero Rch time integral	and non-zero Rch time integral only when fBad 1 or 11	and no occupancy for reasons unknown
May 2002							
337 nm	1281	496	117	121	207	13	327
365 nm	1277	496	117	119	209	11	325
386 nm	1277	496	117	119	209	11	325
420 nm	1277	496	117	119	209	11	325
500 nm	1276	496	117	118	209	11	325
620 nm	1280	496	117	120	209	13	325
Sep 2001							
337 nm	1182	511	151	177	263	1	79
365 nm	1180	511	151	175	263	1	79
386 nm	1180	511	151	175	263	1	79
420 nm	1182	511	151	177	263	1	79
500 nm	1180	511	151	175	263	1	79
620 nm	1182	511	151	177	263	1	79
Sep 2000							
337 nm	938	223	332	159	152	1	71
365 nm	901	223	332	145	123	7	71
386 nm	939	223	332	159	152	1	72
420 nm	906	223	332	146	123	8	74
500 nm	942	223	332	159	152	3	73
620 nm	953	223	332	192	123	2	81

Table 6.2: Detailed accounting of the variety of reasons anterior to data cuts imposed in this analysis that certain PMTs have no fitted efficiency across all wavelengths and all scans

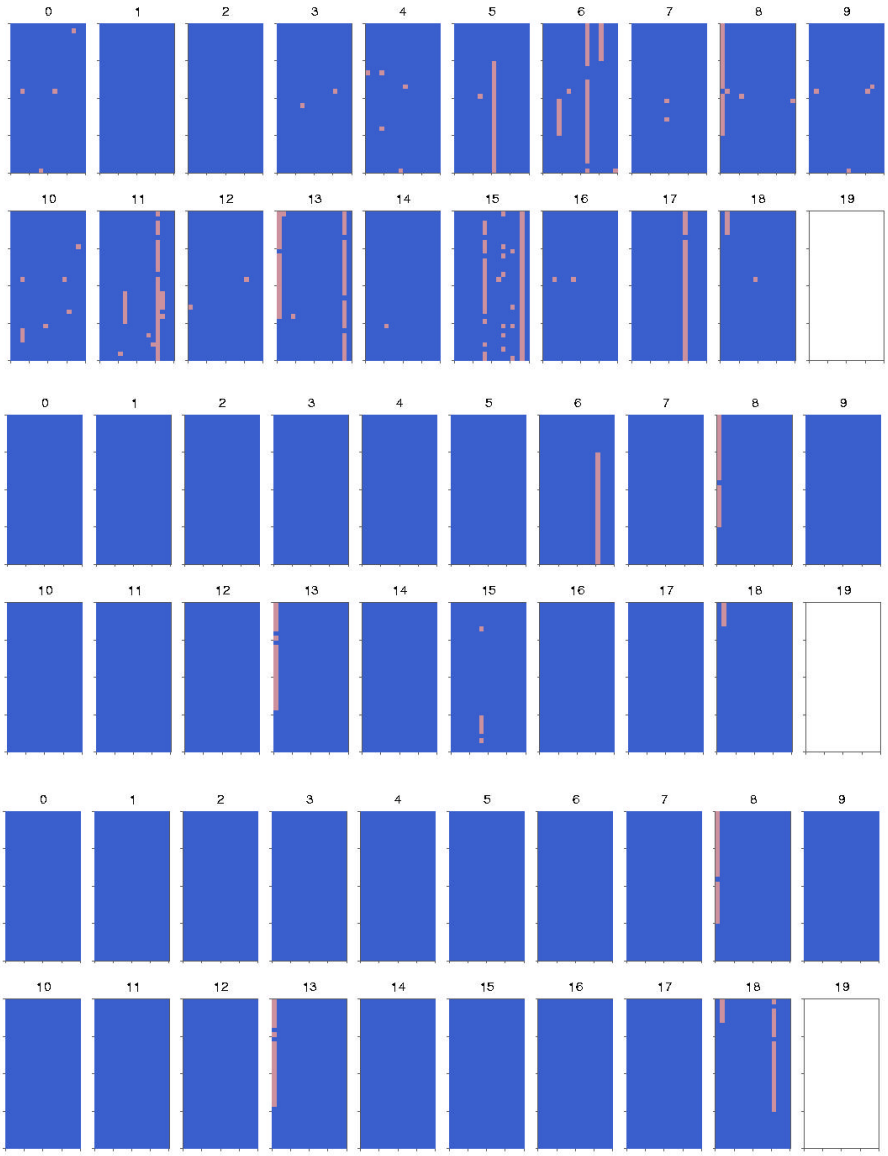

Figure 6.1: The pink dots are a crate map representation of the PMTs which have an Rch Time integral that are not excluded by DQXX, CHCS or fBad equal to 1 or 11. The May 2002 data are the top 19 crates, the September 2001 data the following and September 2000 data are the bottom 19 crates.

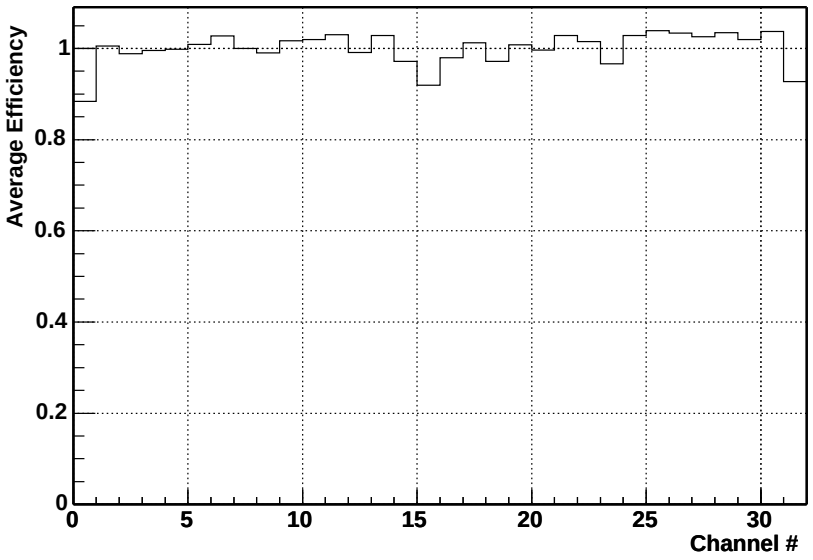

Figure 6.2: Average fitted efficiency as a function of electronics channel number

Another simple influence on efficiency is the voltage that is applied to the PMTs. Even relatively small changes in applied voltage (hundreds of volts compared to thousands) can significantly impact the efficiency of the PMTs and their overall response. For this reason voltage differences are electronically compensated for. As expected, no correlation has been found between a PMT's fitted efficiency and high voltage applied to the PMT as can be seen in figure.6.8. Higher voltage does not mean higher fitted efficiency. Despite variations on the order of 5% found between the fitted efficiency averaged in electronic crates, figure.6.9, no clear correlations can be found. This is likely because the average threshold of the PMTs in the crate for which a fitted efficiency has been found and voltage applied to the crate are not easily disentangled one from another, complicated by the up-down asymmetry in the detector fitted efficiencies.

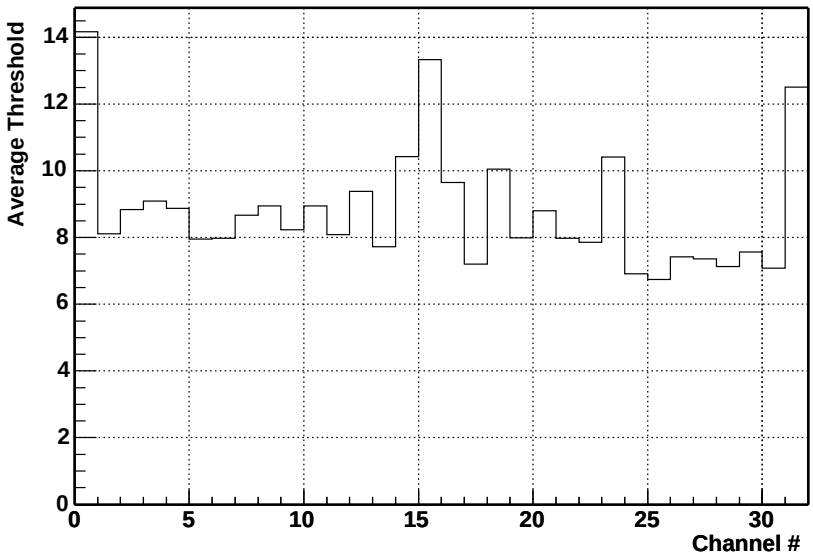

Figure 6.3: Average threshold as a function of electronics channel number

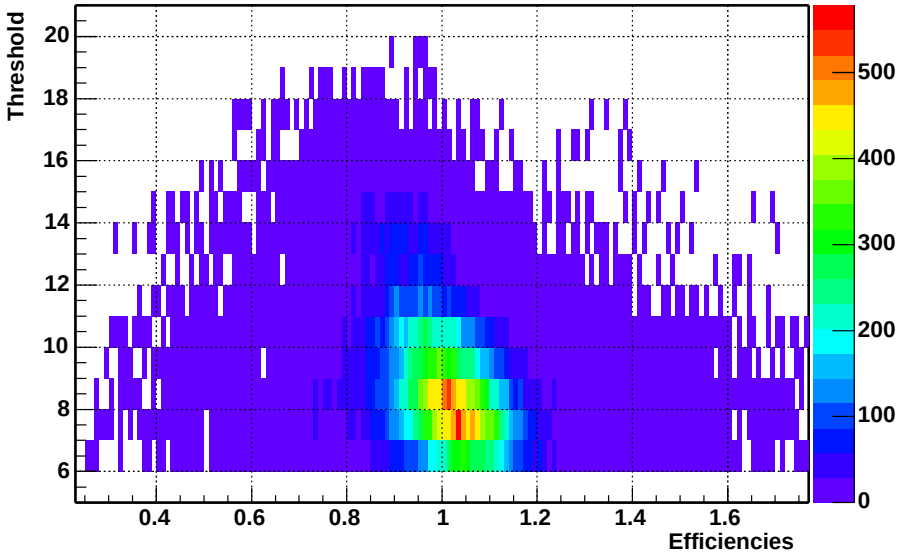

Figure 6.4: Threshold correlation with May 2002 fitted efficiencies

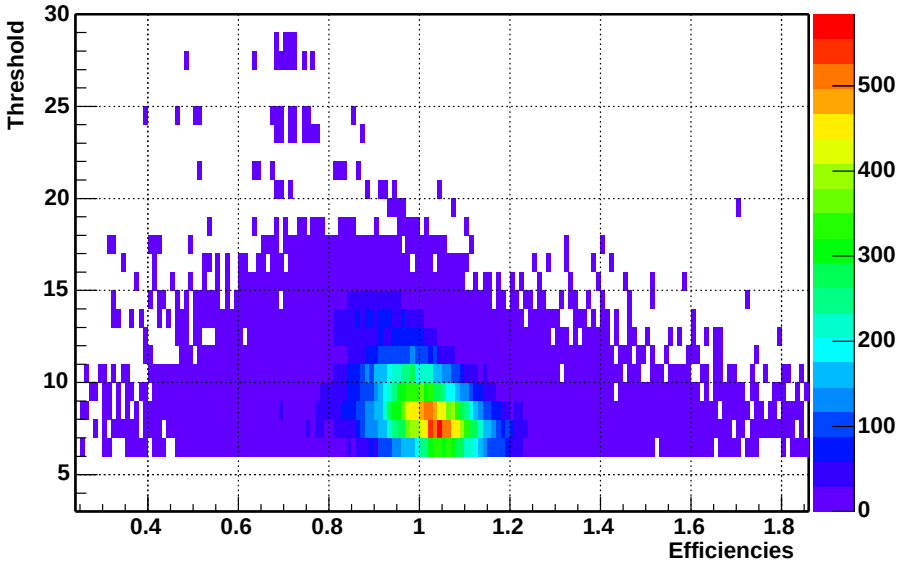

Figure 6.5: Threshold correlation with September 2001 fitted efficiencies

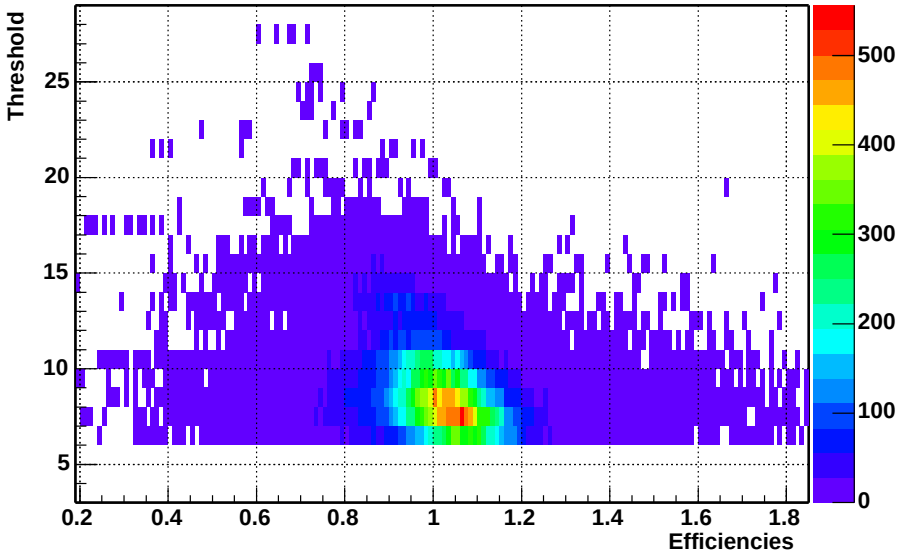

Figure 6.6: Threshold correlation with September 2000 fitted efficiencies

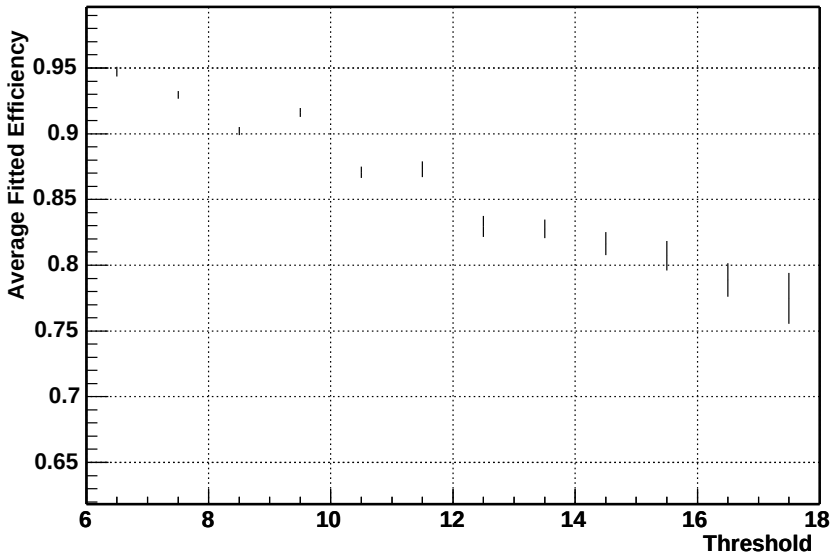

Figure 6.7: Average fitted efficiency as a function of threshold for September 2000 data over all PMTs

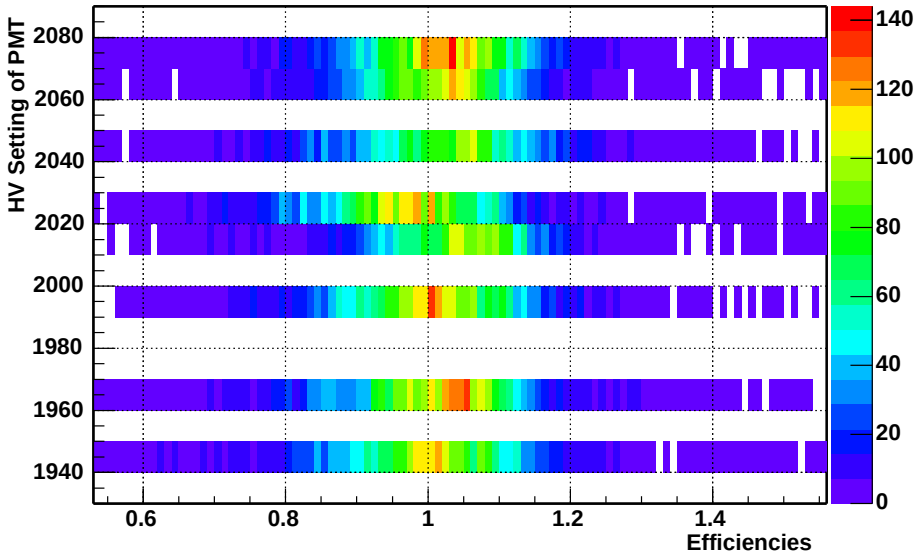

Figure 6.8: No correlation between high voltage and fitted efficiency. There are variations, but higher voltage does not imply higher fitted efficiency

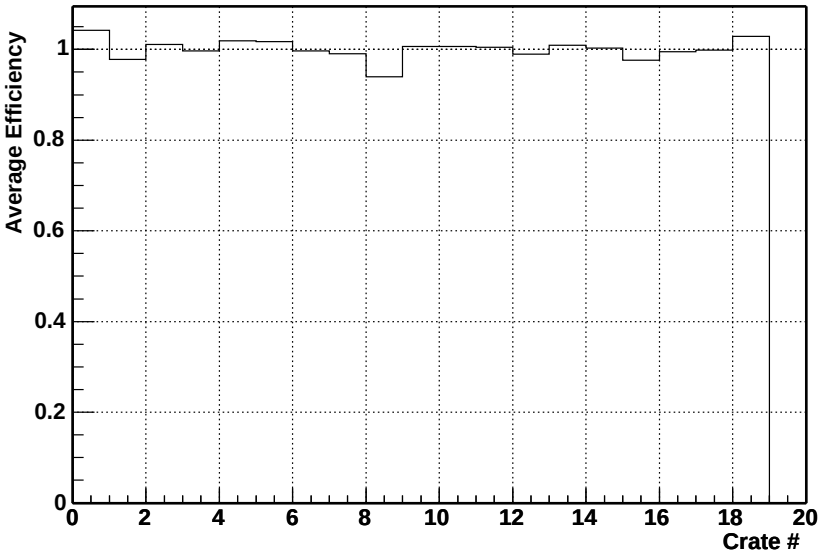

Figure 6.9: Average fitted efficiency as a function of crate number

7. CORRELATION WITH QUEEN'S MEASURED EFFICIENCIES

Before the assembly phase of the construction of the SNO detector the PMTs to be installed were rigorously tested and among the characteristics measured was the quantum efficiency [7]. The efficiencies information was tabulated into a file *spe.txt* with each PMT labeled according to its 4 character bar-code PXXX, where X is a capital letter. The challenge is then to make the correspondence from PXXX into LCN and thus to have LCN vs. efficiency. Another file *ccc_database.dat* holds the bar-codes in LCN ordering so the comparison is readily achieved. Alternatively *database.dat* holds the electronics card numbering scheme, in the form of EXXX, which can be mathematically related back to LCN and this method was also used to confirm the results. Figure.7.1 displays a correlation between the old data and the new. The linear correlation coefficient r between n pairs of observations (x_i,y_i) is defined as

$$r = \frac{\sum_{i=1}^{n}(x_i - \overline{x})(y_i - \overline{y})}{\left[\sum_{i=1}^{n}(x_i - \overline{x})^2 \sum_{i=1}^{n}(y_i - \overline{y})^2\right]^{0.5}}$$

where $\overline{x}$ and $\overline{y}$ are the respective means. "r" ranges between -1 and +1 with values of +1 indicating complete positive correlation, 0 no correlation and -1 complete negative correlation. The linear correlation coefficient for the comparison of the old data and new is 0.983 indicating a strong correlation. The correlation is perhaps not perfect because the old data was taken without the

reflectors that surround the PMTs in the experiment and at different voltage. The two numbering schemes differ by 299 PMTs figure.7.2 which is a direct result of *database.dat* having some PMTs for which no information is available. Since both schemes agree the numbering is certainly correct.

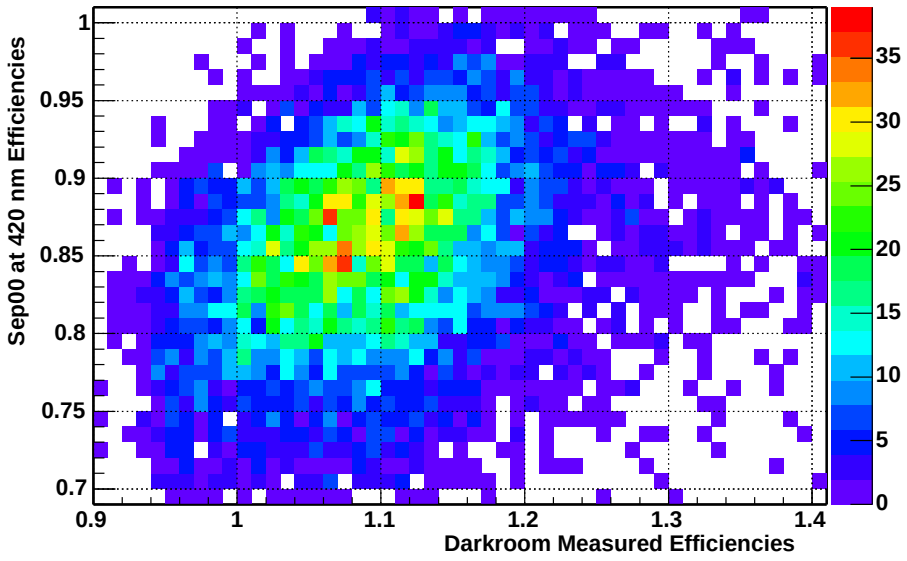

Figure 7.1: Correlation plot of Sep00 at 420nm to Darkroom Measurements

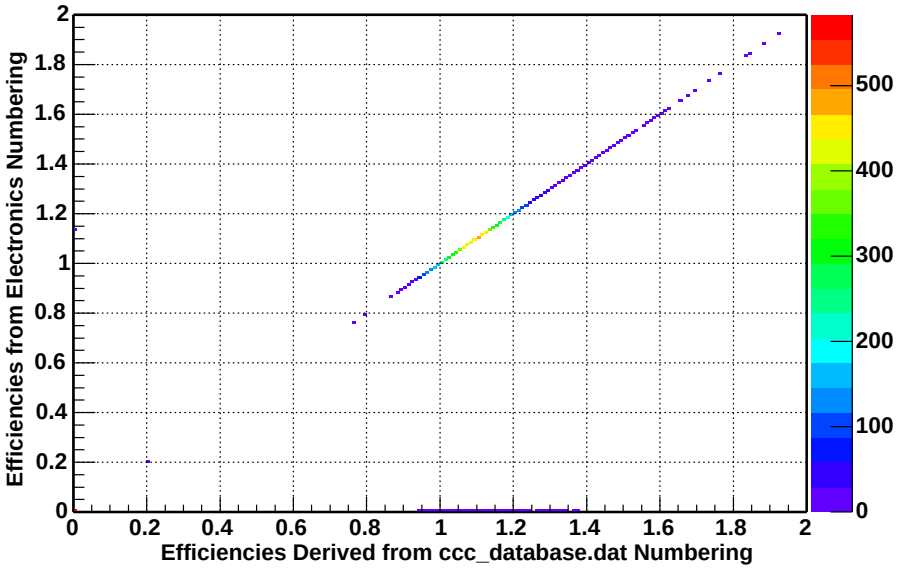

Figure 7.2: Correlation plot to Confirm Accurate Numbering

8. IMPACT ON SNOMAN - THE MONTE CARLO SIMULATION OF SNO

8.1 The Energy resolution discrepancy

To determine the energy resolution and absolute energy scale of the SNO detector the SNO group utilizes a source of radioactive nitrogen gas. ^{16}N decays 4.6% of the time to a 7.12 MeV gamma ray and 66% of the time to a 6.13 MeV beta ray. M.Boulay [4] has noticed a discrepancy between the width of the Monte Carlo (MC) modeled ^{16}N energy distribution and the ^{16}N data energy distribution. The data appears to be always on the order of 1.1 MeV and the MC always on the order of 3% smaller. However the MC used to generate these numbers does not include the PMT to PMT variations. The hope is then that including these variations and the efficiency variability at higher incidence angle that the MC would agree better with data.

8.2 Input of PMT to PMT Variations Into the Monte Carlo

The MC already had built into it the functionality to account for PMT to PMT efficiency differences. The default MC does not use PMT to PMT efficiency differences. The titles files are banks of data that the MC accesses and the *opt_variations.dat* titles file requires no more modification then to input the correct efficiencies into the correct bins. SNOMAN and OCA use different

numbering schemes for PMTs so the first step in the creation of the titles file is to convert LCN to SNOMAN numbering. A simple test to determine that the numbering is indeed correct is to construct a dummy file in which one tube had 100 times the efficiency of all other PMTs and then generate MC data to see if the tube numbers match up - they do. The MC has as default the PMT relative efficiencies turned off. A switch in the code allows them to be turned on. The first step is then to verify that the input efficiencies are indeed having an impact on the MC generated data. The MC simulations performed were photon bomb events, essentially a modeled burst of photons, 2500 photons per event at the specific calibration wavelengths in the center of the detector. The raw occupancy of each PMT is proportional to that PMT's efficiency. The integral of the Rch time profile is proportional to the raw occupancy of the PMT and thus proportional to the efficiency of the PMT. The Rch time integrals for each PMT is tabulated, normalized to the average, and their distribution plotted. This is done for both a MC run with the input PMT to PMT variations in efficiency and one without (a dry run). All MC presented here have the same number of total events.

To verify the efficiencies input are being correctly applied the PMT to PMT ratio of the Rch time profile integrals and the input efficiencies was performed and the resulting distribution generated.

It is clear by the tightening of the distribution that the efficiencies input are impacting the MC as desired. If all of these distributions were purely Gaussian then the sum of the squares of the sigmas should be related. Inputting the PMT to PMT variations should be akin to convolving a Gaussian with a Gaussian. The square of the sigma of the distribution with efficiency variations should equal the square of the sigma of the distribution without efficiency variations summed with the square of the sigma of input efficiency distribution. The MCs were generated with about 9000 events for each PMT. The counting statistics then adjusts these widths by roughly 1.1 percent. $(0.03258 - 0.011)^2 + (0.0778)^2$

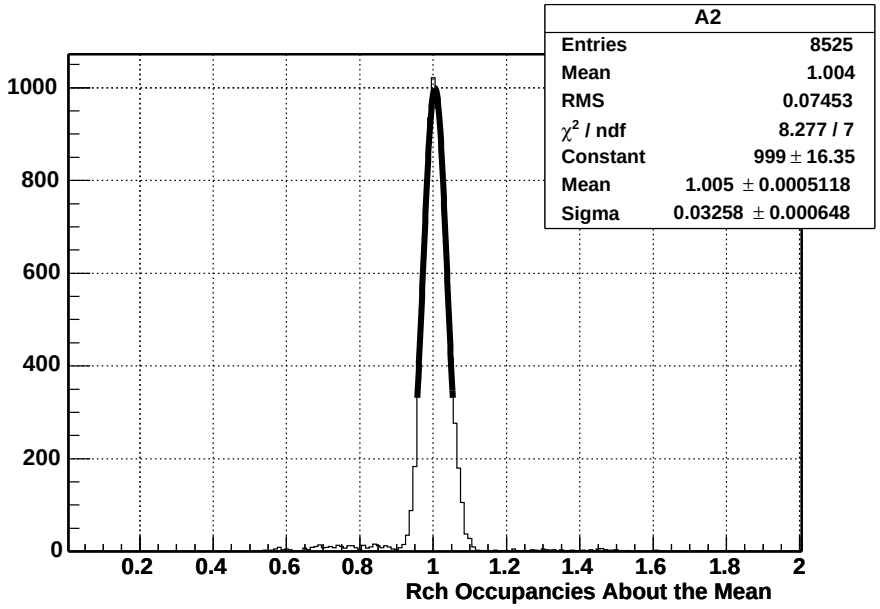

Figure 8.1: MC Laser Data With No PMT to PMT Variations

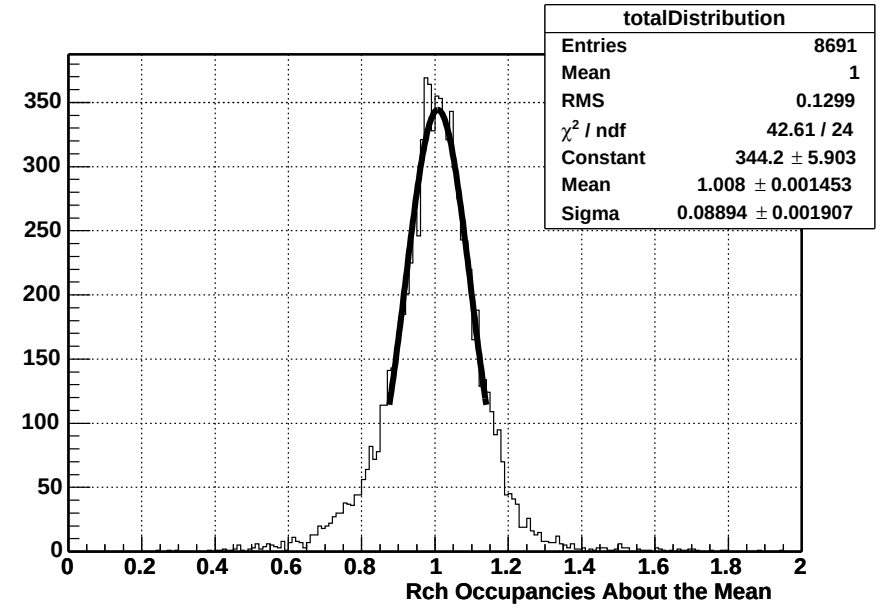

Figure 8.2: MC Laser Data With PMT to PMT Variations

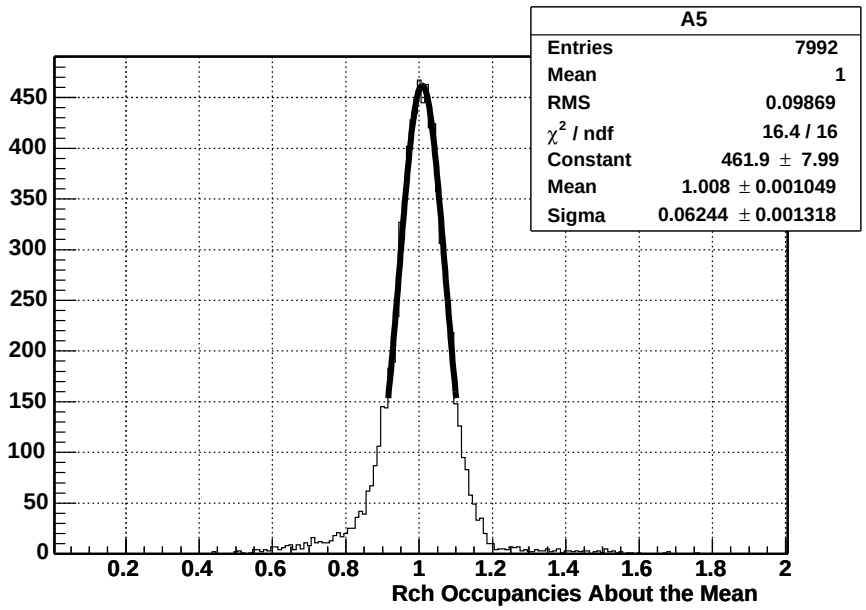

Figure 8.3: MC Laser Data Divided by Input Efficiencies

= 0.006518 should equal $(0.08894 - 0.011)^2 = 0.006074$. They agree to within 6.5% which is acceptable since none of the distributions is purely Gaussian. Furthermore, from the width of the dry run occupancies there appears to be some structure in the MC occupancies above and beyond the input efficiencies, it should be on the order of 1.1%. This is because the PMT angular response is folded into the MC.

8.3 Input of Efficiency Variability with Incidence Angle into the MC

In SNOMAN there was however no existing code for implementing the variability of the efficiencies at higher angles so this was written. A new titles bank was created, AVBL, tabulating the angular variability as a function of 1 degree steps in incidence angle. SNOMAN pmt_vx_pmt.for was modified to implement

the variability. In the unmodified-modified pmt_vx_pmt.for code SNOMAN rejects a number of hits in direct proportion to the efficiency. The modification performed was to first obtain the angle of incidence and wavelength of the impinging photon, then read in the corresponding width from the AVBL banks and then multiply the acceptance efficiency by 1 minus a random number times the AVBL bank width. In other words the efficiency will be spread with increased incidence angle in the exact same way as data does about the fitted efficiency.

One does not expect the additional angular variability to impact central run data significantly whereas off-central data should see a significant effect. Figure.8.4 shows only minimal increase in distribution width caused by folding in the angular variability relative to the previous figure.8.2.

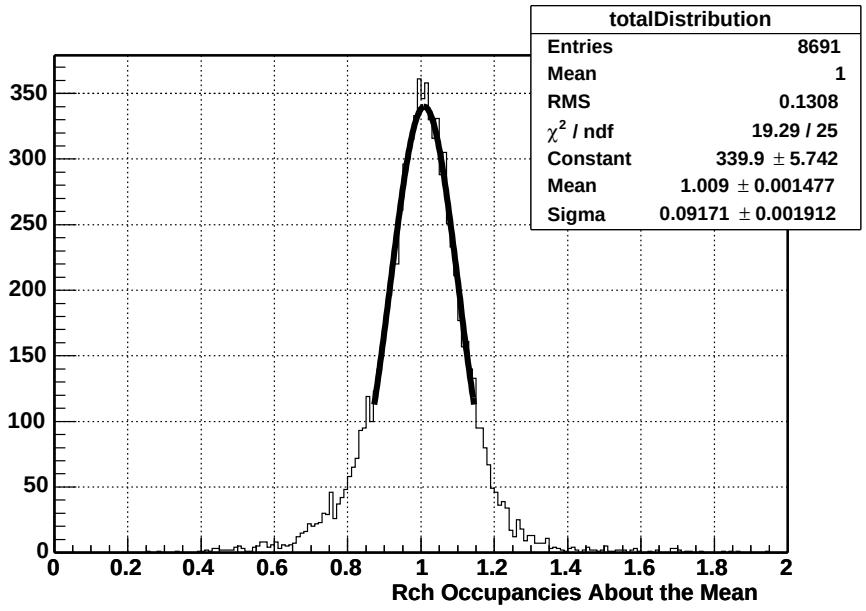

Figure 8.4: MC laser data with PMT to PMT variations and angular variability, laserball at the center of the detector, 420 nm

To simulate off-central data three MC were generated using a "line source". The line source is simply a photon bomb as described earlier but with a random

position along the X-axis of the detector. The effects of the efficiency variability at higher angles can be seen by comparing the Rch time integral distributions for each type of MC, figure.8.5 figure.8.6 and figure.8.7. The Rch time integral distribution gets wider about the mean with inclusion of PMT to PMT variations and wider still with inclusion of the angular variability.

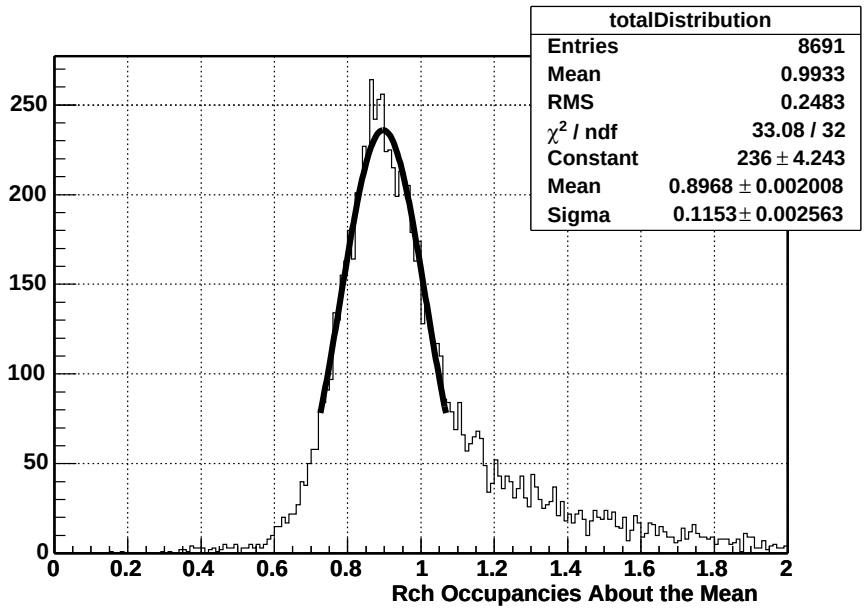

Figure 8.5: MC laser data with PMT to PMT variations and angular variability, line source, 420 nm

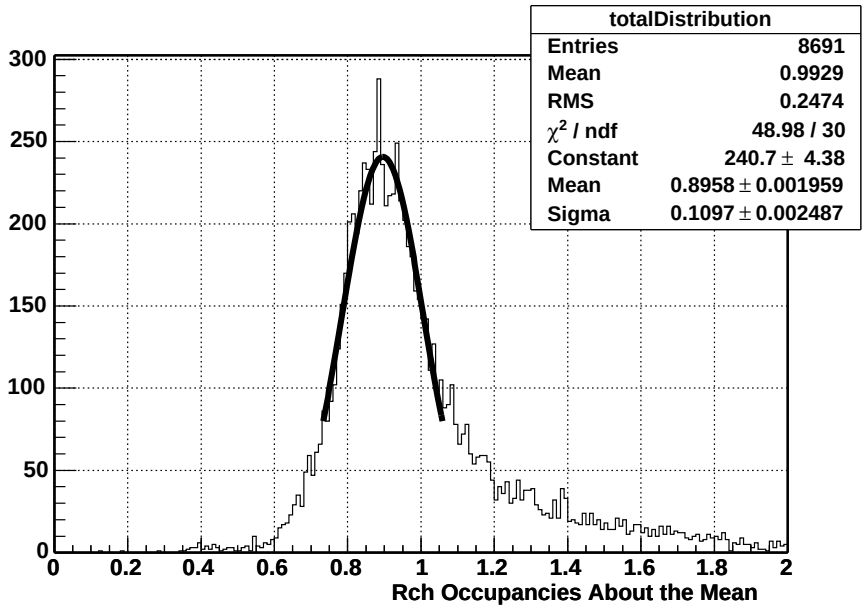

Figure 8.6: MC laser data with PMT to PMT variations and no angular variability, line source, 420 nm

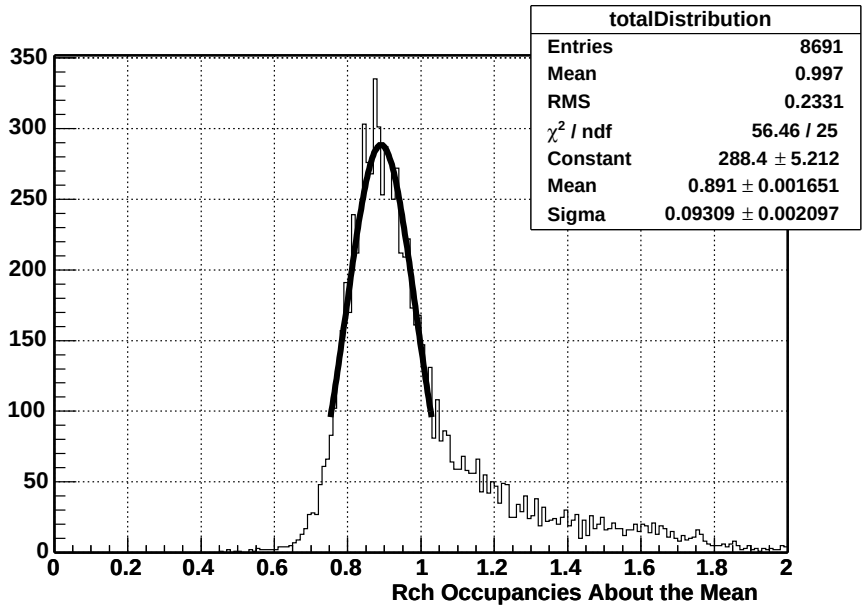

Figure 8.7: MC laser Data without PMT to PMT variations or angular variability, line source, 420 nm

8.4 Correlation with ^{16}N Data and Impact on Energy Resolution

The most fundamental cross-check to validate the analysis of efficiencies that can be performed is perhaps to compare efficiency information extracted from laserball data to the efficiency information garnered from a completely different source, ^{16}N. Fitted efficiency from the May 2002 laserball scan at 420 nm and ^{16}N occupancy data for a near to central run were compared on a PMT to PMT basis in a correlation plot, figure.8.8. Furthermore it is shown in figure.8.9 that there is no correlation between PMT fitted efficiency and ^{16}N MC without PMT to PMT variations. There is however as expected a correlation between PMT fitted efficiency and ^{16}N MC with PMT to PMT variations, figure.8.10. The correlations between ^{16}N data occupancies and both types of ^{16}N MC, with and without PMT variations, can be seen in figure.8.11 and figure.8.12. Finally the distributions of occupancies can be seen in figure.8.13. The (sigma;mean) for the fits are as follows: Data = (0.000423;0.003779), MC with PMT to PMT variations = (0.0005627;0.003774) and default MC = (0.0003467;0.003765). There were 788 Data events per PMT on average, 183 per PMT on average in both MC. After factoring out statistics for the the distributions the widths are as follows: Data = 0.1061, MC with PMT to PMT variations = 0.1294 and MC without PMT to PMT variations = 0.0553. PMT variations. The adjustments made by inputing the PMT to PMT variations appear to be a little over-compensating. There are a few potential reasons for this: 1) the MC is generated at the center but the data file used, which was the best one available at the time, is 10 cm off in the Z-direction. 2) as of the time of writing this thesis the MC is known to model the N16 source incorrectly. The spatial distribution of events generated does not currently match with source distribution. 3) the MC has a history of exaggerating the effect of poorly modeled PMTs in and around belly plates and ropes.

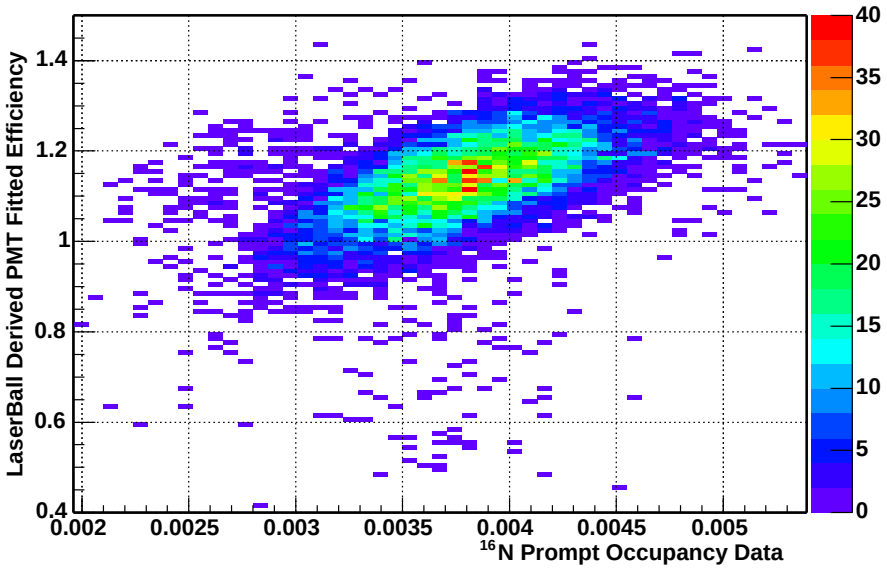

Figure 8.8: Correlation between PMT fitted efficiency taken from laserball data and PMT occupancy taken from ^{16}N data

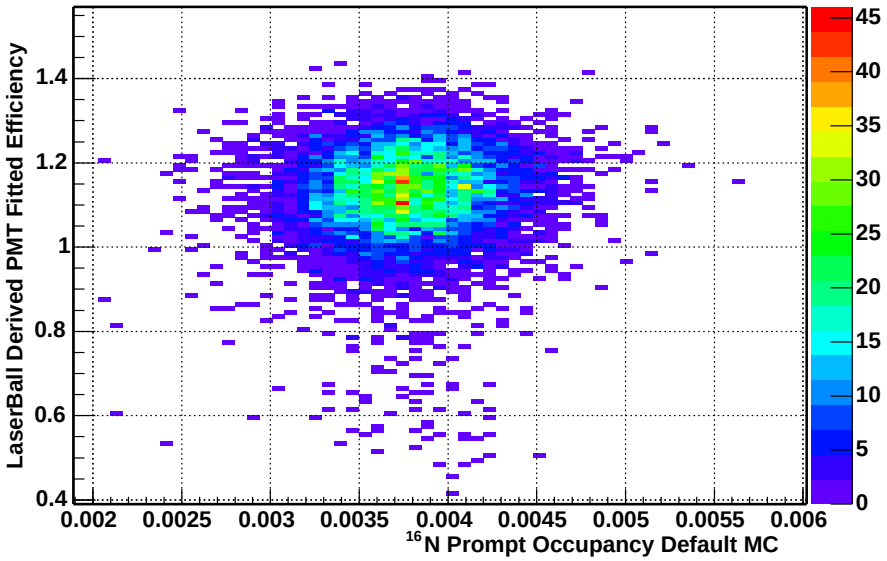

Figure 8.9: No correlation exists between ^{16}N MC PMT occupancy without PMT to PMT variations and PMT fitted efficiencies from laserball data

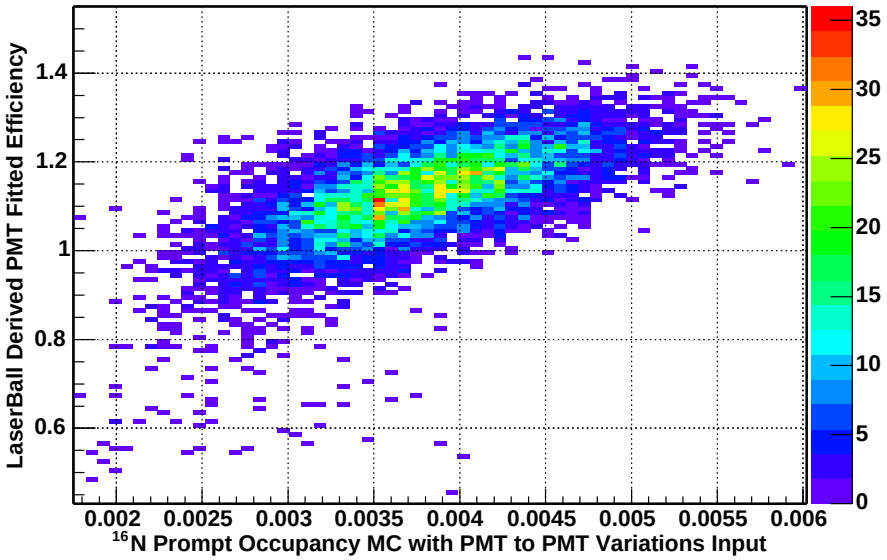

Figure 8.10: Correlation between PMT fitted efficiency taken from laserball data and ^{16}N MC PMT occupancy with PMT to PMT variations input

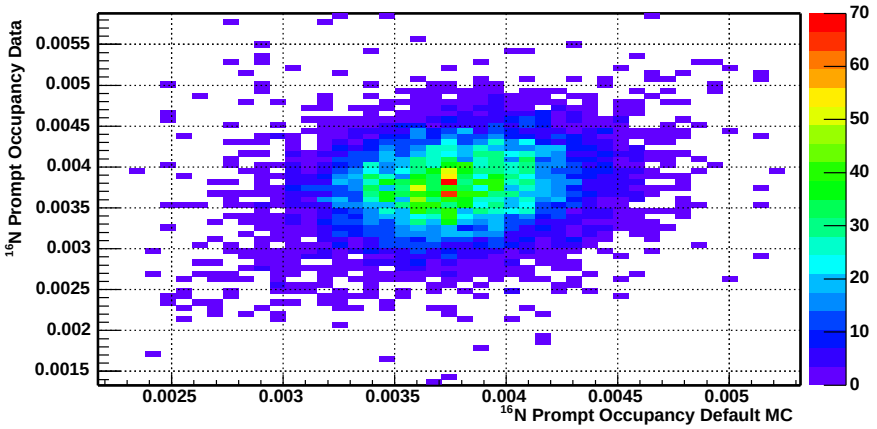

Figure 8.11: No correlation exists between ^{16}N MC PMT occupancy and ^{16}N data PMT occupancy

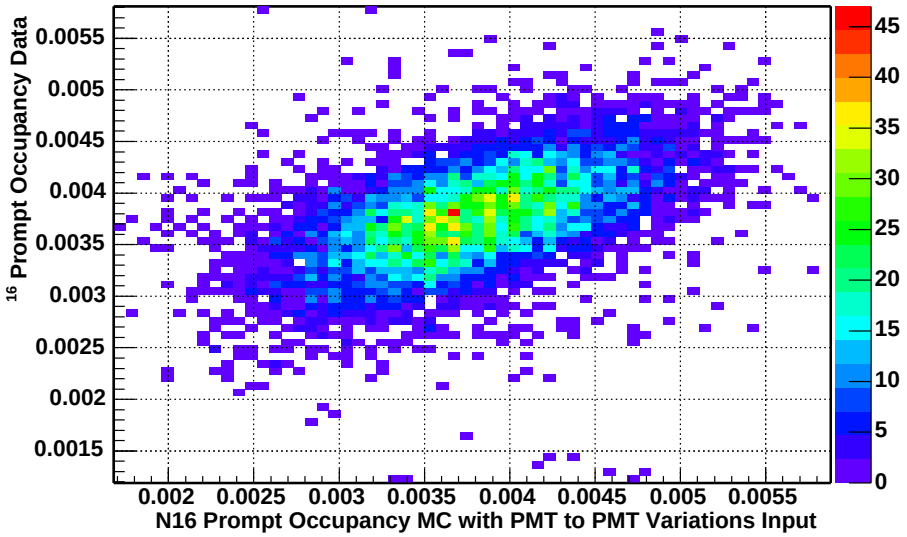

Figure 8.12: Correlation between ^{16}N MC PMT occupancy with PMT to PMT variations input and ^{16}N data occupancy

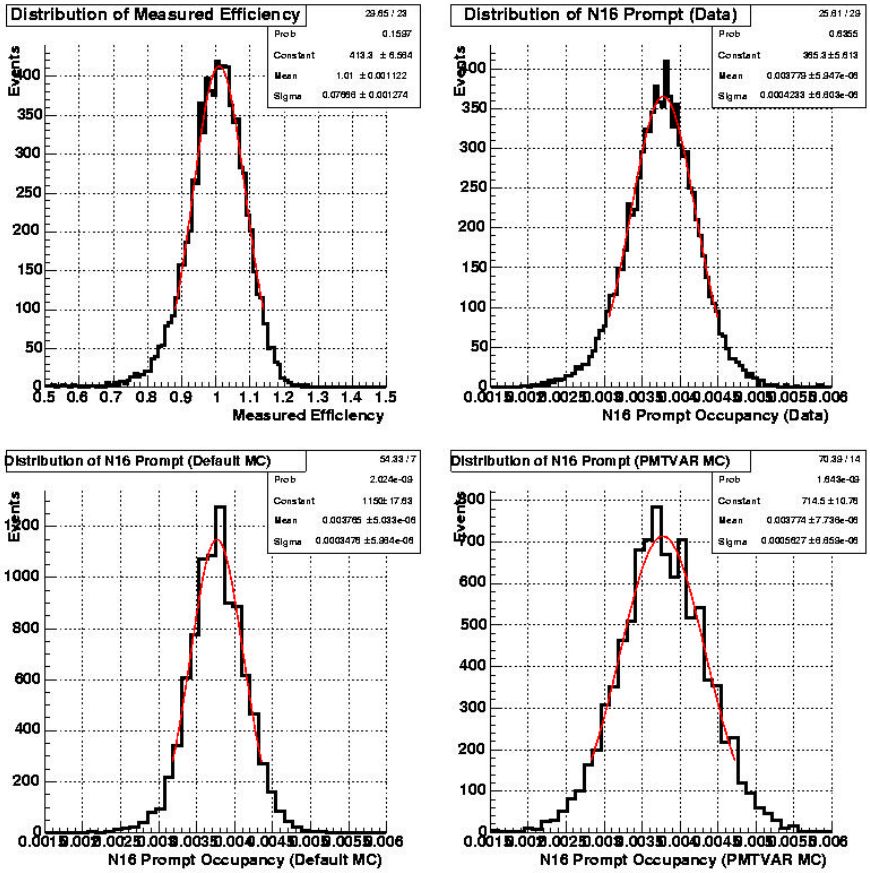

Figure 8.13: Occupancy distributions of ^{16}N data, MC without PMT to PMT variations and MC with PMT to PMT variations

9. CONCLUSION

This thesis is the first study to investigate local variations in PMT efficiencies in SNO. The results of the thesis confirm the PMT efficiencies are quite stable relative to each other. The top half of the detector has been found to be slightly less efficient than the bottom half. PMT efficiency has been shown to be more variable with greater angle of incidence of light in a quantified, seemingly random way. Input of the PMT to PMT efficiency variations into the MC has demonstrated better agreement of the MC with data.

The background counts SNO receives are primarily from decays in the Uranium and Thorium chains, from the rock that surrounds the detector. This background peaks at lower energies than the 5 MeV threshold through which all data are filtered. The extraction of neutrino fluxes however hinges significantly on a good understanding of the background tail above the 5 MeV threshold. While a small change in the energy resolution of each event is not likely to impact the fluxes in any significant way, a small change in the resolution of the very large background tail CAN impact the fluxes, at least the error on the fluxes. Since the background tail used in the extraction of neutrino fluxes is modeled by the SNOMAN Monte-Carlo there is reason to believe that the results of this thesis may further constrain the neutrino fluxes.

REFERENCES

1. B. Moffat. *The Optical Calibration of the Sudbury Neutrino Observatory.* PhD thesis, Queen's University, Kingston, Ontario, Canada, 2001.

2. R.J. Ford. *SNO N_2/Dye Laser and Fibre Optic Diffuser Ball System Manual.* Queen's University, 1997. SNO-STR-96-056.

3. M.G. Boulay *Direct evidence for Weak Flavor Mixing with the Sudbury Neutrino Observatory.* PhD thesis, Queen's University, Kingston, Ontario, Canada, April 2001.

4. M.G. Boulay *RSP and the Unified Analysis* Internal report. 2001.

5. Phil Harvey *XSnoed* August 2001 http://manhattan.sno.laurentian.ca/xsnoed/

6. R. Brun and F. Rademakers. ROOT - An object oriented data analysis framework. *Nuclear Instruments and Methods*, A389:81-86, April 1997. URL http://root.cern.ch

7. C.J. Jillings et al. The photomultiplier tube testing facility for the Sudbury Neutrino Observatory. *Nuclear Instruments and Methods*, A373:421-429, January 1996.

8. J. Bodger et al. The Sudbury Neutrino Observatory. *Nuclear Instruments and Methods*, A449:172-207, July 2000.

9. SNO Collaboration. *The SNOMAN User's Manual*, 4.01 edition, November

2000. SNO collaboration internal refrence manual. Released periodically with updates.

VITA

Name:	Christian Van Ouellet
Place and Year of birth:	Ottawa, 1979
Education:	Queen's University, 1997-2001
	BScH SSP Astrophysics 2001
Experience:	Research assistant, Queen's SNO group
	Summer of 2000 and 2001